Geophysical Journal International

Geophys. J. Int. (2016) **205,** 395–413
GJI Geodynamics and tectonics

doi: 10.1093/gji/ggw022

Plate kinematics of the central Atlantic during the Oligocene and early Miocene

Antonio Schettino[1] and Chiara Macchiavelli[1,2]

[1]*School of Science and Technology – Geology Division, University of Camerino, Via Gentile III da Varano, I-*62032 *Camerino (MC), Italy.*
E-mail: antonio.schettino@unicam.it
[2]*Institute of Earth Sciences Jaume Almera, ICTJA-CSIC, Lluis Sole i Sabaris s/n, E-*08028 *Barcelona, Spain*

Accepted 2016 January 15. Received 2016 January 14; in original form 2015 September 14

SUMMARY

A new plate motions model for the northwest Africa–North America Plate pair during the Oligocene and early Miocene is presented. The model is accompanied by a high-resolution isochron map for the central Atlantic region, resulting from a re-examination of 423 ship tracks from the NGDC data base for the area between the 15°20′ FZ and the Azores triple junction. A new digital model of fracture zones for this region and a set of 309 magnetic profiles crossing the Oligocene to recent oceanic crust within the study area allowed to determine accurate finite reconstruction poles for the North America–northwest Africa conjugate plate pair between the early Miocene (Chron 6) and the early Oligocene (Chron 13). For times older than Chron 7 (∼25 Ma), the finite reconstruction poles were calculated using a reliable data set coming exclusively from the region south of the Canary Islands FZ (∼32°N), which allowed to test the rigidity of the northwest African oceanic lithosphere during the Oligocene–early Miocene phase of Atlas orogeny. A comparison of theoretical magnetic isochrons with observed magnetic lineations systematically shows that anomalously high spreading rates occurred in the area north of the Canary Islands FZ before Chron 7, thereby suggesting that the formation of the Atlas mountain, rather than being a localized intracontinental process, was logically linked to the central Atlantic spreading history. Thus, an independent Moroccan Plate could have existed during the Oligocene–early Miocene time interval, which included both the oceanic lithosphere north of the Canary Islands FZ and the northern Maghrebian areas of Morocco, Algeria and Tunisia. In this eventuality, the Atlas mountain belt should be reinterpreted as a giant flower structure associated with dextral transpression.

Key words: Plate motions; Magnetic anomalies: modelling and interpretation; Marine magnetics and palaeomagnetics.

1 INTRODUCTION

Although the kinematics of the central Atlantic region has been studied extensively since the 1960s (Heirtzler *et al.* 1968; Le Pichon & Fox 1971; Pitman & Talwani 1972; Francheteau 1973; Sclater *et al.* 1977; Olivet *et al*. 1984; Klitgord & Schouten 1986; Sundvik & Larson 1988; Roest *et al*. 1992; Schettino & Turco 2009; Labails *et al.* 2010; Merkouriev & DeMets 2014), the complexity of the ridge processes that occurred in this area during the Cenozoic has raised a series of intriguing questions that are still waiting for a satisfactory answer. For example, several V-shaped structures can be observed around the mid-Atlantic Ridge (MAR), which are uncommon along other oceanic spreading centres. These features have been interpreted alternatively as minor fracture zones (Rona 1976; Rona & Gray 1980), traces of volcanic segments that propagate along the plate boundary as a consequence of asthenospheric axial flow (Schouten *et al.* 1987; Müller & Roest 1992), traces of melting anomalies associated with ridge–plume interaction (Vogt 1971; White 1997; Escartín *et al.* 2001; Jones *et al.* 2002). Another unsolved problem is represented by the formation of the Atlas mountain belt in northwest Africa, which has been generally considered either as an Alpine chain (i.e. related to the convergence between Africa and Eurasia, e.g. Hafid *et al.* 2006) or as an intracontinental mountain range that experienced moderate crustal shortening and exhumation as a result of crustal isostatic and dynamic topography (e.g. Teixell *et al.* 2003). To date, only a few authors have debated these mainstream interpretations, either on the basis of kinematic (Schettino & Turco 2009; Schettino *et al.* 2010) or geological (Malusà *et al.* 2007; Ellero *et al.* 2012) evidence.

In this study, we present the first high-resolution kinematic model of the central Atlantic for the time interval comprised between the early Oligocene and the early Miocene, with the objective to help

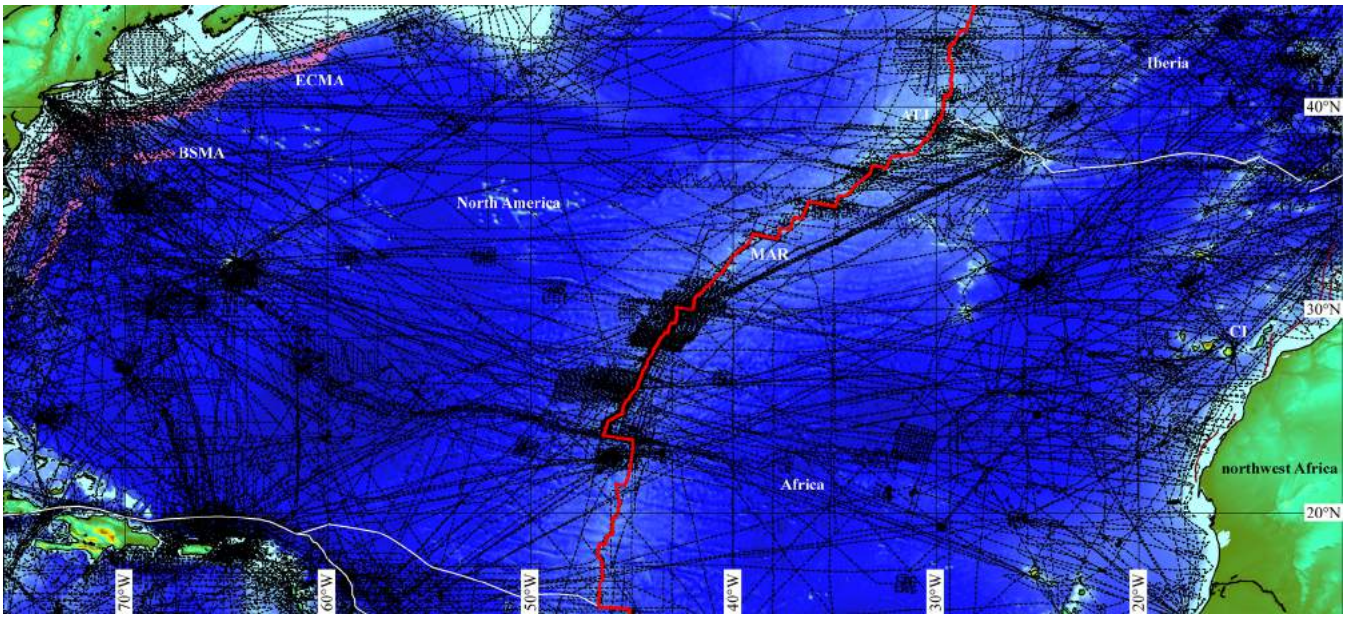

Figure 1. Study area, showing available ship-track data from the GEODAS–NGDC (black dashed lines). ECMA, East Coast Magnetic Anomaly; BSMA, Blake Spur Magnetic Anomaly; CI, Canary Islands.

understanding the processes that occurred in this region during the last 33 Myr. In particular, we are going to test if the oceanic lithosphere to the east of the MAR behaved as a single northwest African Plate, as assumed in the classic models, or alternatively that a separate Moroccan Plate existed during the Oligocene–early Miocene as suggested by Schettino & Turco (2009). A second objective is to investigate the possibility that simple ridge kinematics may provide an alternative explanation for the observed V-shaped structures. Finally, we want to test if secondary tectonic stages existed, associated with changes in plate motions, during the time interval between the early Oligocene and the early Miocene within the 'canonical' stages bounded by anomalies 13 (33.1 Ma), 8 (25.8 Ma) and 6 (20.1 Ma; e.g. Müller *et al.* 1999).

The study area includes the oceanic lithosphere between 15°N and the Azores triple junction (ATJ; Fig. 1). We used marine magnetic data from 423 ship tracks in the NGDC data base to determine magnetic anomaly picks, and the latest version (ver. 23) of the global free-air gravity anomaly map (Sandwell *et al.* 2014) to create an accurate digital model of fracture zones (Fig. 2). The resulting data set of magnetic anomaly crossings and fracture zones was used in the inversion algorithms to obtain finite reconstruction poles for North America with respect to northwest Africa and to generate a new isochron map for the central Atlantic.

The formation of the Atlas mountain belt requires that northwest Africa was subject to some amount of internal deformation during the Cenozoic. Therefore, it is of paramount importance to establish whether or not it behaved as a single quasi-rigid plate during the Oligocene–early Miocene time interval. When this research started, shortly after the publication of a paper from Schettino & Turco (2009) and the subsequent debate about the existence of an independent Moroccan Plate (Labails *et al.* 2010; Schettino *et al.* 2010), a high-resolution isochron chart for the central Atlantic region had not yet been published. However, a recent comprehensive study from Merkouriev & DeMets (2014) has produced a detailed plate motions model between Nubia and North America since Anomaly 6. Consequently, our results for times younger than Chron 6 are briefly presented here only for completeness. For the time interval between chrons 6 and 13, the results discussed in this study represent the first attempt to describe accurately both ridge processes and plate motions in the central Atlantic region. We shall see that the magnetic evidence suggests the existence of an independent Moroccan Plate, because all the available magnetic profiles north of the Canary Islands FZ (CIFZ) show higher spreading rates for times older than Anomaly 7 (~25 Ma), which correlates with the timing of the Atlas orogeny. Therefore, the model presented here supports the possibility that the CIFZ was temporarily converted into a right-lateral strike-slip plate boundary during the Cenozoic, allowing eastward escape of an independent Moroccan Plate.

2 FRACTURE ZONES OF THE CENTRAL ATLANTIC REGION

In addition to magnetic anomaly crossings, quantitative determination of the seafloor spreading history of an oceanic basin requires an accurate identification of transform faults and fracture zone trends, because these features constrain Euler pole locations in the inversion procedure. As mentioned above, we used the recent global free-air gravity anomaly map of Sandwell *et al.* (2014) to digitize fracture zone segments in the central Atlantic (Fig. 2). In the resulting digital model, four active V-shaped structures were assumed to be composed by oblique alignments of small abandoned transform faults, according to the process described below. Therefore, they were included in the compilation as lineations formed by small fracture zone segments. However, these data did not participate to the inversion procedure for determining finite reconstruction poles, because only sampling points from the large-offset fracture zones were used for that purpose.

It is well known that V-shaped structures around spreading ridges originate from spot features of the newly forming oceanic lithosphere, which shift longitudinally along the axial zone (either northwards or southwards in the case of the MAR). In the north Atlantic and Azores region, these structures assume the form of narrow ridges that start at the axial zone and are disposed symmetrically

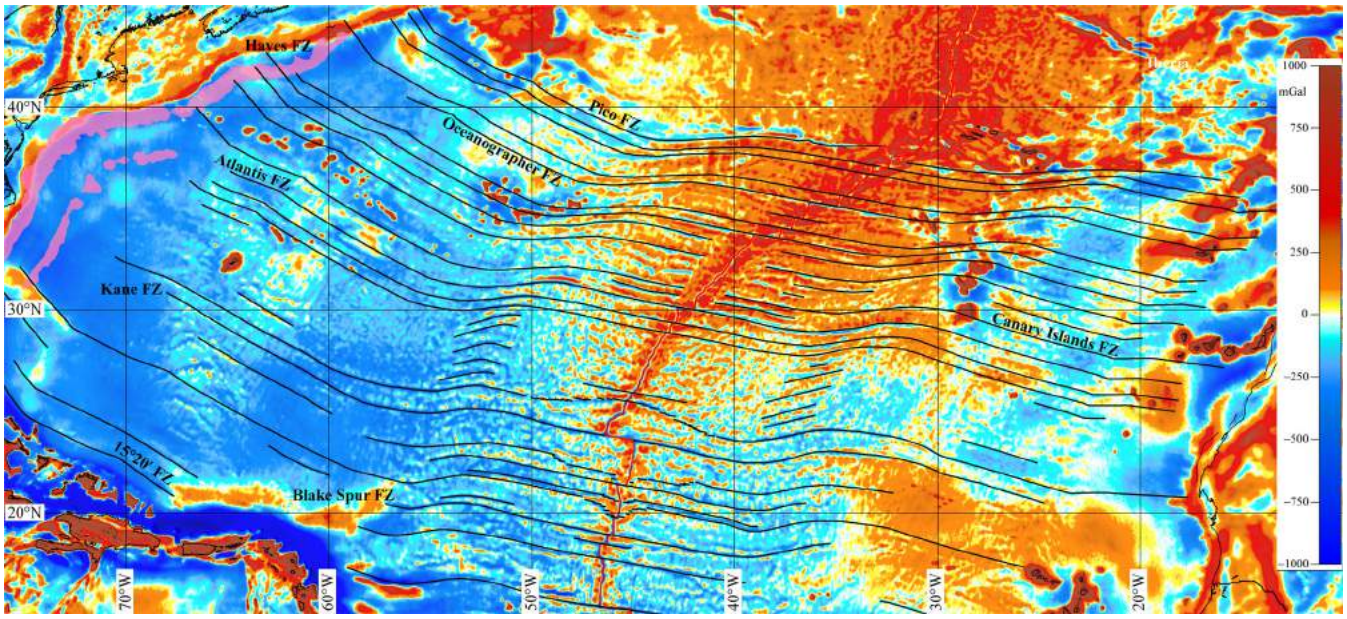

Figure 2. Central Atlantic fracture zones, identified on the basis of gravity anomaly data (black lines). The background raster shows free-air gravity anomalies (Sandwell *et al.* 2014).

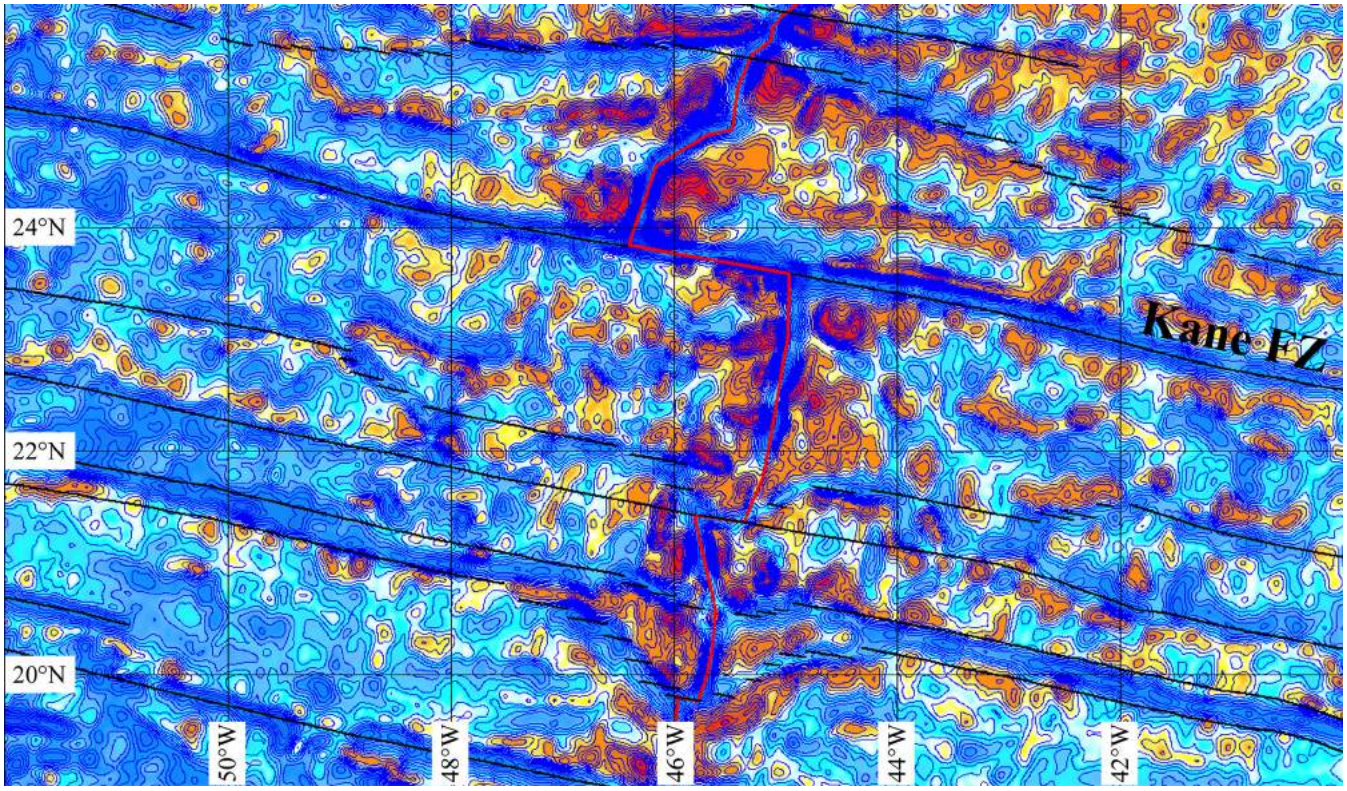

Figure 3. Active V-shaped structures in the central Atlantic.

about the spreading centre (Gente *et al.* 1995; Escartín *et al.* 2001; Jones *et al.* 2002). Their geometry suggests that they are associated either with flow of hot spot material or melting regime anomalies that migrate at high velocity, up to 122 mm yr^{-1} around Iceland. Conversely, the active V-shaped structures that can be observed between 19°N and 26°N in the central Atlantic are depressions rather than ridges, which form large angles with the axial zone (Fig. 3). In this instance, the velocity of migration along the axial zone is rather low, ranging between 2.7 and 5.2 mm yr^{-1}. Furthermore, and most importantly, they always appear in combination with interrupted fracture zones. In fact, Figs 2 and 3 show four fracture zones that terminate at the outer ends of corresponding V-shaped structures without reaching the spreading ridge. These observations led us to postulate that the central Atlantic V-shaped structures were

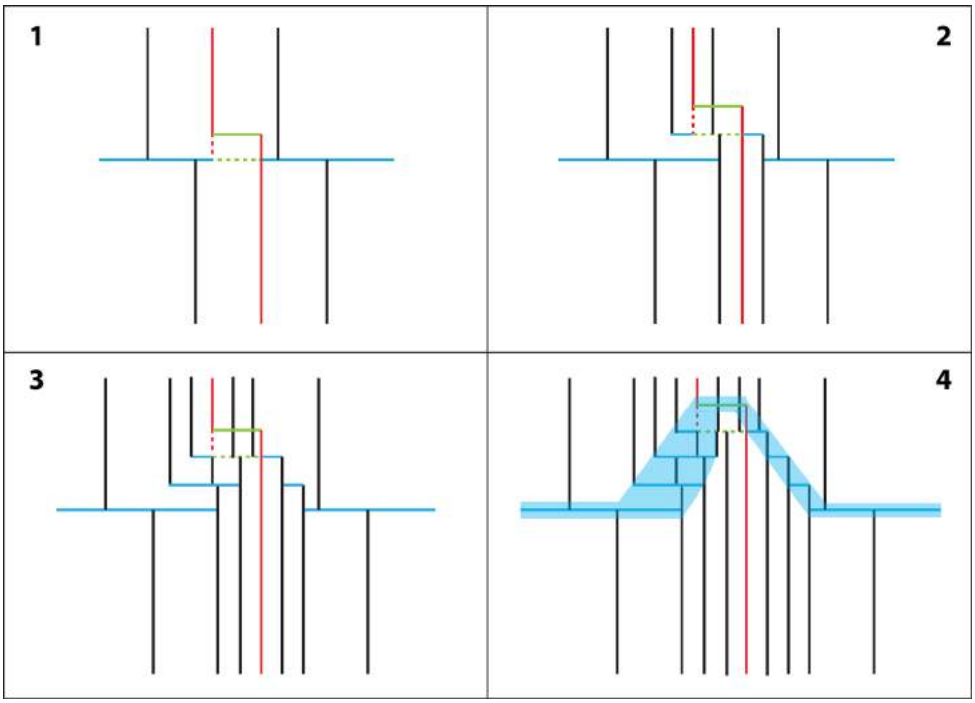

Figure 4. Hey's (1977) model of formation of V-shaped structures. Blue lines, fracture zones; Red lines, spreading segments; Green lines, transform faults; Black lines, isochrons. In (1), the small-offset transform fault linking to spreading segments is abandoned after an eastward ridge jump of the southernmost part of the northern segment, which allows to the southern segment to propagate northwards. The process is repeated in (2–3) by additional ridge jumps of the dooming end of the northern segment, which resolve into a northward propagation of the southern segment. The resulting pattern of fracture zones assumes the form of a V-shaped structure as shown in (4).

associated with fracture zones as suggested by Kleinrock *et al.* (1997), in agreement with the general mechanism of axial ridge propagation first proposed by Hey (1977).

In Hey's (1977) model, small-offset transform faults play a critical role. In principle, these structures can migrate along the axial zone through a series of ridge jumps, as illustrated in Fig. 4. At some time, the terminal part of one of the two spreading segments linked by a small-offset transform fault is abandoned, while the other segment propagates across the older offset fault. The resulting spreading ridge geometry does not include overlapping segments, because a new small-offset transform fault forms, which links the propagating end of one segment with the active end of the dooming segment.

Although many fossil V-shaped structures can be observed in the central Atlantic, which could be associated with small-offset transform fault kinematics (Kleinrock *et al.* 1997), we mapped only the four structures that are still active along the present day MAR (Fig. 2). However, an accurate inspection of the gravity anomalies shows that a future extension of the isochron map to times older that 33 Ma (Anomaly 13) will require a complete digital model of these features across the oceanic lithosphere of pre-Oligocene age.

Starting from the south, the digital compilation of fracture zones illustrated in Fig. 2 includes six large-offset fracture zones, namely the 15°20′, Kane, Atlantis, Hayes, Oceanographer, and Pico FZs, eleven smal-offset fracture zones, plus four pseudo-fracture zones associated with a sharp change in strike of the spreading ridge. In addition, some fracture zones between the Hayes and Atlantis FZs become extinct between Chrons 4 and 5B, whereas others formed as a consequence of ridge jumps. With respect to previous fracture zone maps for the central Atlantic (Klitgord & Schouten 1986; Müller *et al.* 1999; Matthews *et al.* 2011), Fig. 2 includes a more accurate representation of the trends close to the North American margin, which are representative of the initial directions of spreading during the early Jurassic (Schettino & Turco 2009).

3 SEAFLOOR SPREADING ANOMALIES

From the 423 ship tracks in the NGDC data base for the central Atlantic, we extracted 309 magnetic profiles crossing the Oligocene to recent oceanic crust (Fig. 5). The magnetic anomalies were recalculated using appropriate DGRFs and *Kp* index profiles were generated to assess data quality. All the magnetic profiles were high-pass filtered to remove unwanted long wavelength components and to obtain zero-average trend-free profiles. The interpretation of the 309 magnetic profiles was performed using *Magan*, an interactive computer program for forward-modelling developed by Schettino (2012). To calculate model anomalies, we set the declination, $D_0(\boldsymbol{r},t)$, and inclination, $I_0(\boldsymbol{r},t)$, of the geomagnetic field at any point $\boldsymbol{r}$ along the magnetic profiles at survey time t through DGRF models. The thickness of the magnetized layer was set to 0.5 km in all cases. For each block in a magnetization model, the direction of remnant magnetization was calculated using the APW paths of Schettino & Scotese (2005). Finally, the upper surface of the magnetized sources was assumed to be coincident with bathymetry. In this study, we considered 17 magnetic anomalies, from Anomaly 2A to Anomaly 13, to build a plate motions model between northwest Africa and North America. The correlation points of these anomalies, which were assigned ages according to the geomagnetic polarity time scale of Cande & Kent (1995), are shown in Fig. 6. Such correlation points usually coincide with the young edge of the corresponding chrons, with the exception of anomalies 5 and 6, for which we followed the convention adopted by previous authors (e.g. Müller *et al.* 1997), who assigned the anomaly to the boundary

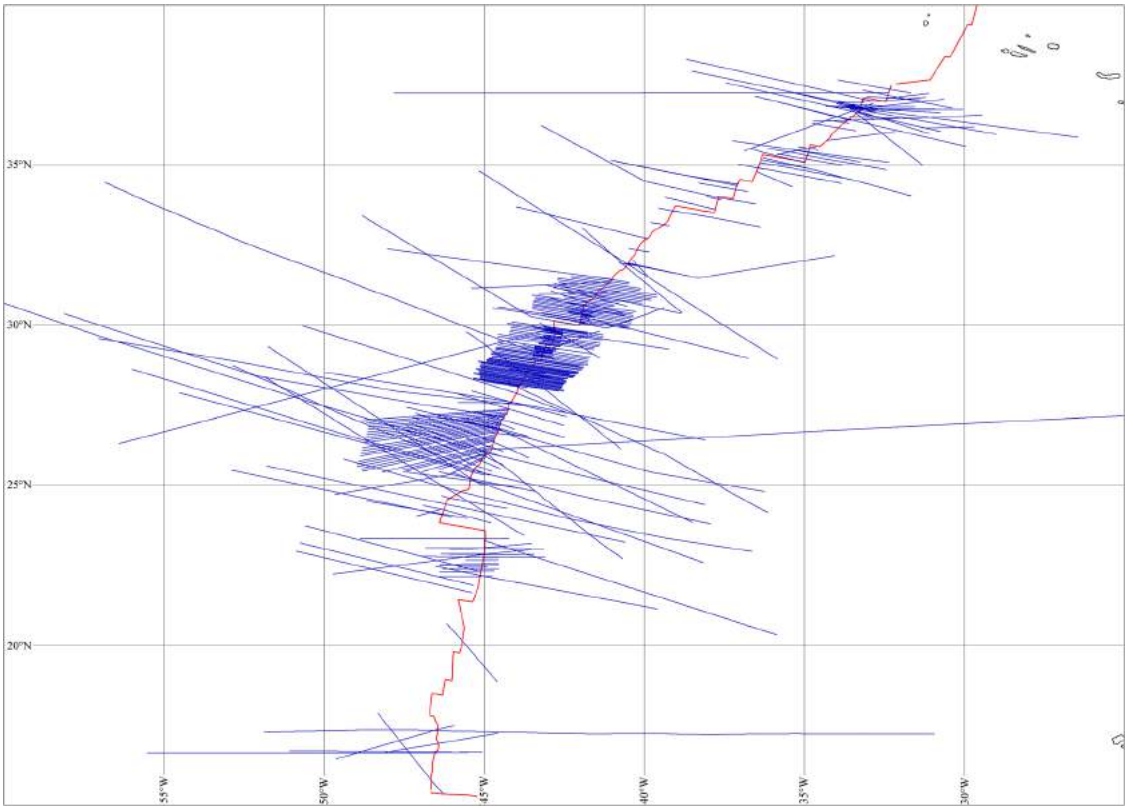

Figure 5. Traces of magnetic profiles used in this study (blue lines).

between the main normal and reversed polarity chrons. A correlation chart for the whole set of 309 magnetic profiles, showing the alignment of identified anomalies around the MAR, can be found in the supporting information.

Fig. 7 shows the distribution of magnetic crossings for the selected anomalies, which were used in conjunction with fracture zone data to determine finite Euler rotations of North America relative to northwest Africa at anomaly times. These results are listed in Table 1. The best estimate of 1σ random noise in anomaly picking varies between 2.5 and 4.1 km. It is important to note that wide areas in the central Atlantic have poor coverage of anomaly crossings, notably below 23°N and above 32°N. As a consequence, finite reconstruction poles for anomalies older than Anomaly 5 are constrained by a much lower number of spreading ridge segments, as indicated by the dramatic decrease in degrees of freedom (DOF) for the Euler rotations older than 11 Ma in Table 1. We used an improved version of Hellinger's algorithm (Hellinger 1981), included in the software PLACA (Matias *et al.* 2005), to determine finite reconstruction poles for anomalies 2A, 3, 3A, 4, 5, 5B, 5C, 5D, 5E, 6, 6B, 7, 8, 9, 10, 12 and 13. Fig. 8 shows the superposition of magnetic anomaly crossings and crossings reconstructed using the best-fitting rotations listed in Table 1. These data were used to build magnetic lineations and isochrons according to standard procedures (e.g. Schettino 2014). The resulting isochron chart for the central Atlantic since Anomaly 13 is shown in Fig. 9. It illustrates the ridge processes that occurred in this region starting from 33 Ma. For example, it is possible to note the coalescence of four spreading segments to form a single linear ridge between 31°N and 34°N after Anomaly 5 or, alternatively, the split of a ridge segment to form two distinct spreading segments separated by a transform fault around 34°N at anomaly 5 time (~11 Ma). More to the south, the map illustrates the effect of the axial migration of small-offset transform faults described in the last section. Finally, we can observe several episodes of formation of pseudo-fracture zones as a consequence of localized variations of spreading asymmetry (e.g. just south of 25°N or around 28°N).

Starting from Anomaly 8, the finite reconstruction poles listed in Table 1 were calculated excluding crossings from the region north of the CIFZ, in order to test the rigidity of northwest Africa during the Oligocene–early Miocene phase of Atlas orogeny. This test could not be performed determining rotation parameters directly from crossings observed in the region comprised between 30°N and the ATJ, because the available data set was too sparse to allow a reliable statistical estimation of rotation parameters. Consequently, in the isochron chart of Fig. 9, isochron segments north of the CIFZ from Anomaly 8 to Anomaly 13 are substituted by representative magnetic lineations.

The rotation parameters listed in Table 1 can be used to generate velocity fields and create base maps for plate reconstructions. However, if they are used to predict local spreading rates and compare the results with observed values, it is necessary to correct for both spreading asymmetry and outward displacement. An estimate of the spreading asymmetries associated with the isochron map of Fig. 9 is listed in Table 2. The asymmetry (α) was calculated by the following formula:

$$\alpha = \frac{2\Delta x_E}{v\Delta t} - 1, \tag{1}$$

where Δx_E is the distance (in km) between two isochrons along the eastern side of the spreading ridge in the case of stage asymmetry, or the distance of an isochron from the ridge in the case of average asymmetry. In eq. (1), v is the full spreading rate (in km Myr^{-1}) while Δt is the time interval between two isochrons or the age of an isochron. The quantity α is positive when the width of the

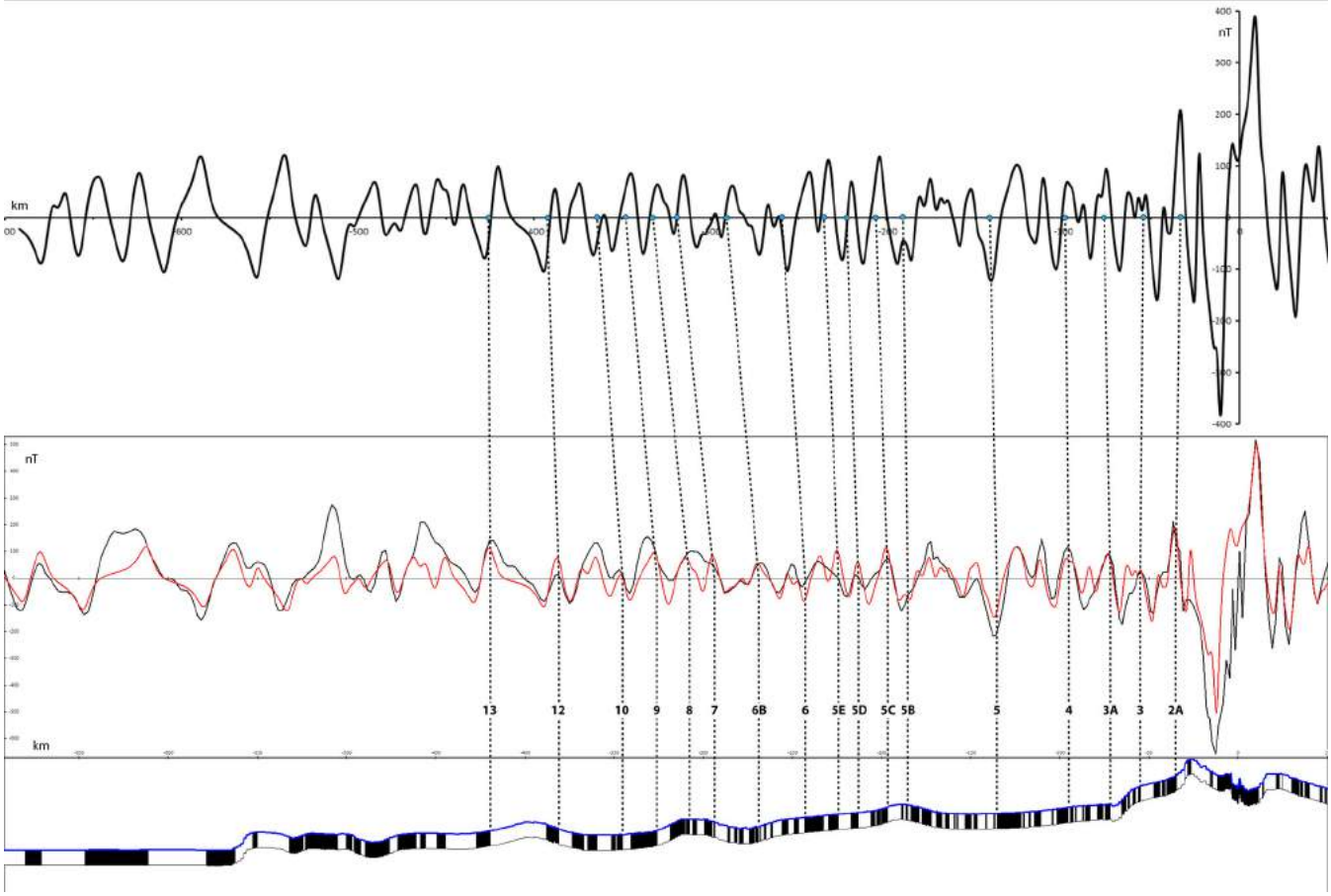

Figure 6. Correlation points of magnetic anomalies. The lower panel shows the best fitting magnetization model and anomaly locations associated with an observed magnetic profile (middle panel – black line). The red line shows the theoretical magnetic signal generated by such magnetization distribution. The upper panel shows a constant-velocity model, obtained using the average full spreading velocity of the best-fitting model between anomaly 13 and the present.

crust accreted to the African side during some time interval Δt exceeded the width of the crust accreted to the North American side. From Table 2, we note that the overall spreading asymmetry since Anomaly 13 increased from ∼–10 per cent at the northern segment to ∼0 per cent at the southernmost segment and that this trend is reproduced for the stage between anomalies 6 and 13. Therefore, the relative amount of crust that was accreted to North America since the Oligocene is higher in the northern part of the central Atlantic, so that the corresponding MAR segments were displaced eastwards with respect to the southern segments.

In order to compare the spreading velocities predicted using the kinematic parameters listed in Table 1 with GPS data or other kinematic models of current plate motions in the central Atlantic, we need to correct the Euler pole relative to the stage (0–2A) for outward displacement (DeMets & Wilson 2008). An overall estimate can be obtained introducing the angular outward displacement, $\delta\Omega$, which is the intercept of the best-fitting linear function of angular displacements Ω versus time t:

$$\Omega(t) = kt + \delta\Omega. \quad (2)$$

In this expression, k is the slope of the linear regression curve $\Omega = \Omega(t)$ determined by stage poles. In this study, we had just two stage boundaries at anomalies 2A ($t_1 = 2.58$ Ma) and 3 ($t_2 = 4.18$ Ma), and corresponding stage angles $\Omega_1 = 0.56^\circ$ and $\Omega_2 = 0.34^\circ$. Therefore, the slope resulted to be $k = 0.2125^\circ$ Myr^{-1}. Hence, from (2) we easily obtain: $\delta\Omega = 0.0118^\circ$. This is the angular correction that should be applied to the most recent Euler pole in Table 1. In terms of linear distances, at the northern and southern ends of the MAR we have: $\delta x_{\min} \cong 1.14$ km $\delta x_{\max} \cong 1.30$ km, respectively. These results are in agreement with the estimates of DeMets & Wilson (2008) and Merkouriev & DeMets (2014). In terms of spreading rates, we obtain respectively $v_{\min} \cong 20.67$ mm yr^{-1} and $v_{\max} \cong 23.61$ mm yr^{-1} at the northern and southern ends of the MAR, instead of $v_{\min} \cong 21.04$ mm yr^{-1} and $v_{\max} \cong 24.04$ mm yr^{-1} as calculated from the rotation model in Table 1.

4 PLATE MOTIONS AROUND THE CENTRAL ATLANTIC SINCE THE OLIGOCENE

Confidence ellipses for the rotation poles listed in Table 1 are shown in Figs 10 and 11. We note that the confidence ellipse of Anomaly 3 is entirely included in the Anomaly 2A region of uncertainty. Therefore, it is not possible to distinguish, on a statistical basis, the stages 0–C2A and C2A–C3. Even taking into account of the angular velocities, they form a single stage that spans the last 4.18 Myr. With the exception of Anomaly 5, the remaining Euler poles form a quite regular westward directed arrangement. Fig. 12 shows a plot of the minimum and maximum spreading rates along the central Atlantic ridge. Of course, the maximum rate corresponds to the most distal point along the spreading ridge relative to the stage

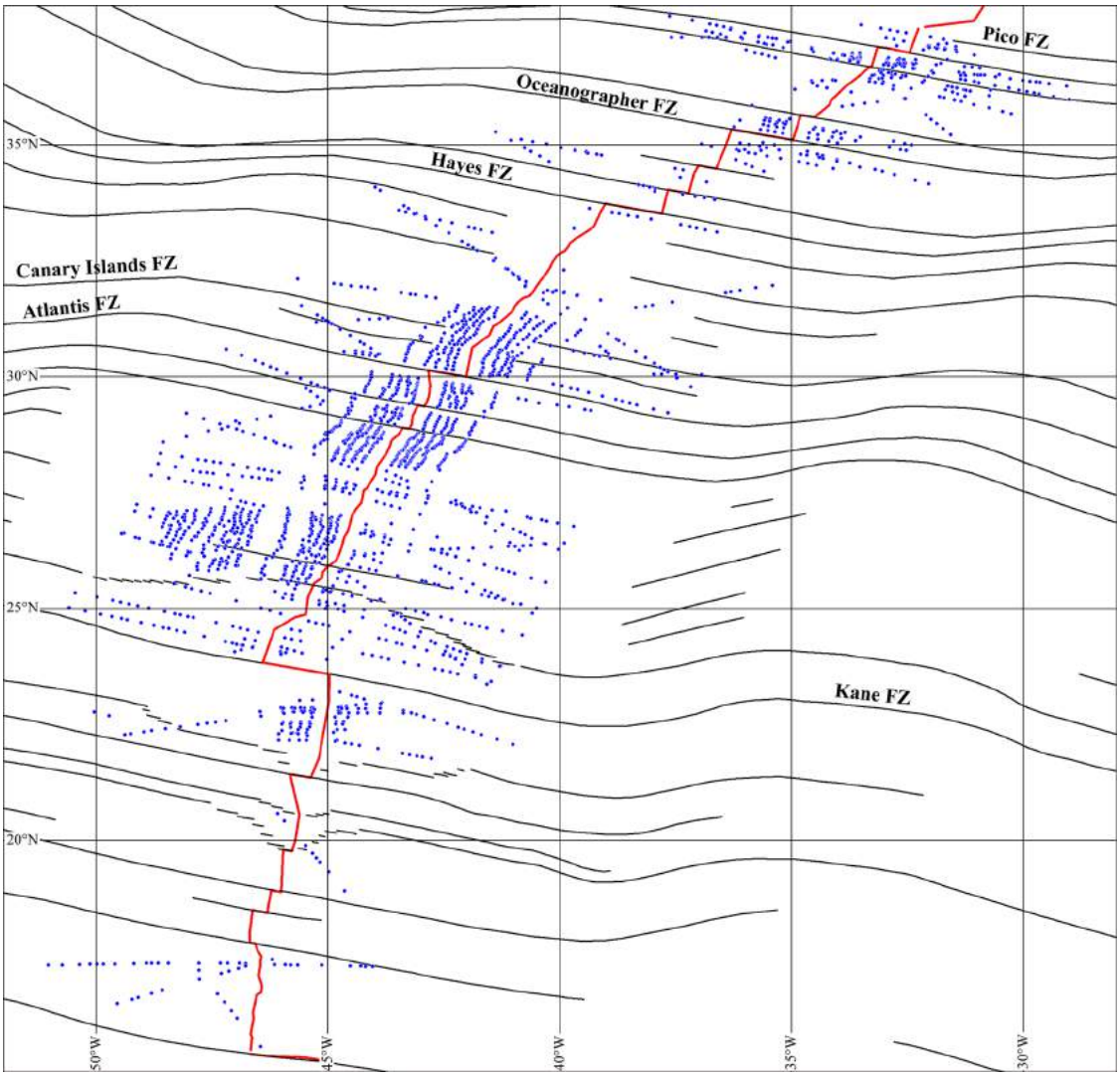

Figure 7. Distribution of magnetic anomaly crossings for anomalies 2A (2.58 Ma), 3 (4.18 Ma), 3A (5.89 Ma), 4 (7.43 Ma), 5 (10.95 Ma), 5B (14.80 Ma), 5C (16.01 Ma), 5D (17.28 Ma), 5E (18.28 Ma), 6 (20.13 Ma), 6B (22.59 Ma), 7 (24.73 Ma), 8 (25.82 Ma), 9 (27.03 Ma), 10 (28.28 Ma), 12 (30.48 Ma) and 13 (33.06 Ma) (blue dots).

pole. This graph is much more informative of an angular velocity plot, because angular velocities may change also in absence of real spreading rate variations. In fact, they may change simply as a consequence of variations in the stage pole location, even in the case of an approximately constant spreading rate. The plot in Fig. 12 shows that the difference between maximum and minimum velocity decreases with time, especially after 23 Ma. This indicates that the stage poles corresponding to the finite reconstructions listed in Table 1 have progressively moved away from the MAR. Regarding the average spreading rate, it was subject to six major transitions at Anomaly 10 (28.28 Ma), 6 (20.13 Ma), 5D (17.28 Ma), 5C (16.01 Ma), 5 (10.95 Ma) and 4 (7.43 Ma), with a sharp velocity drop at the last stage boundary. Starting from 7.4 Ma (Anomaly 4), the average spreading rate varies between 23 and 24 mm yr^{-1}.

In the northern part of the central Atlantic, an important feature of the magnetic crossings associated with anomalies older than Anomaly 7 is represented by a systematic mismatch with corresponding rotated crossings. In fact, the latter are invariably displaced toward the MAR by 30–35 km with respect to the conjugate magnetic lineations. Fig. 13 shows the example of Anomaly 8 crossings. Although the data set north of the CIFZ is incomplete and cannot be used to determine reliable reconstruction poles, stage poles, and angular velocities for ages older than ∼25 Ma, the observed misfit of crossings is indicative of the fact that the spreading rates in this area could have been higher than that predicted by the southern data set. Six high-quality magnetic profiles from this area are illustrated in Figs 14(a)–(f). They show that the observed crossings for anomalies 8–13 are systematically displaced landwards from both sides of the MAR with respect to theoretical crossings obtained from the rotation parameters of Table 1, the latter being constrained only by magnetic data south of the CIFZ. Therefore, the magnetic evidence suggests the possibility that an independent tectonic plate formed during the Oligocene in the northern part of the central Atlantic, at the expense of either the North American or the northwest African Plate. In the former case, the western branch of the CIFZ was temporarily converted into a sinistral strike-slip fault and compressional structures formed along the North American margin. In the alternative scenario, the eastern branch of this fracture zone was converted into a dextral strike-slip fault and compressional structures formed in northwest Africa (see fig. 6 in Schettino & Turco

Table 1. Finite reconstruction poles and covariance matrices of N. America relative to northwest Africa.

N	Anomaly	Age (Ma)	λ (°)	φ (°)	Ω (°)	δ*x* (km)	*A*	*b*	*c*	*d*	*e*	*f*
547	2A	2.58	75.94	89.35	0.56	4.0	2.348	–2.077	0.010	2.213	–0.010	0.000
449	3	4.18	76.01	88.41	0.90	2.5	5.255	–4.472	0.032	4.598	–0.032	0.000
357	3A	5.89	78.92	73.83	1.30	3.8	5.263	–2.316	0.031	1.631	–0.018	0.000
325	4	7.43	79.34	64.43	1.68	3.0	1.172	–0.430	0.017	0.181	–0.006	0.000
260	5	10.95	78.38	77.13	2.55	3.0	3.026	–1.846	0.060	1.270	–0.039	0.002
48	5B	14.80	79.65	54.87	3.80	3.6	0.836	–0.162	0.028	0.063	–0.006	0.001
72	5C	16.01	79.76	54.10	4.15	2.6	2.792	–0.778	0.099	0.332	–0.031	0.005
70	5D	17.28	79.75	53.36	4.48	3.2	2.583	–0.296	0.088	0.174	–0.013	0.005
64	5E	18.28	79.80	47.47	4.80	4.2	5.631	–0.167	0.235	0.252	–0.013	0.013
70	6	20.13	79.73	41.29	5.40	3.8	2.590	0.207	0.109	0.152	0.006	0.006
51	6B	22.59	79.62	42.39	6.03	3.1	2.325	0.146	0.131	0.083	0.006	0.009
61	7	24.73	79.14	29.04	6.78	3.2	3.883	1.087	0.293	0.355	0.082	0.024
37	8	25.82	77.88	14.52	7.31	3.3	0.677	0.335	0.050	0.282	0.025	0.006
54	9	27.03	77.36	11.01	7.74	3.3	2.142	1.262	0.216	0.814	0.128	0.024
31	10	28.28	76.41	5.24	8.24	3.0	0.638	0.472	0.071	0.453	0.055	0.010
45	12	30.48	75.33	0.66	9.11	3.9	0.953	0.801	0.141	0.763	0.123	0.026
33	13	33.06	73.76	–4.98	10.25	2.8	0.407	0.412	0.077	0.480	0.082	0.018

Notes: N represents the degrees of freedom (total number of anomaly and fracture zone crossings minus twice the total number of anomaly and fracture zone segments minus 3. (λ,φ) are latitude and longitude of reconstruction poles, Ω are rotation angles (ccw positive). δ*x* is the 1σ uncertainty on crossing location in the spreading direction. Elements *a*, *d* and *f* are diagonal elements of the variance–covariance matrix, while *b*, *c* and *e* represent off-diagonal components;

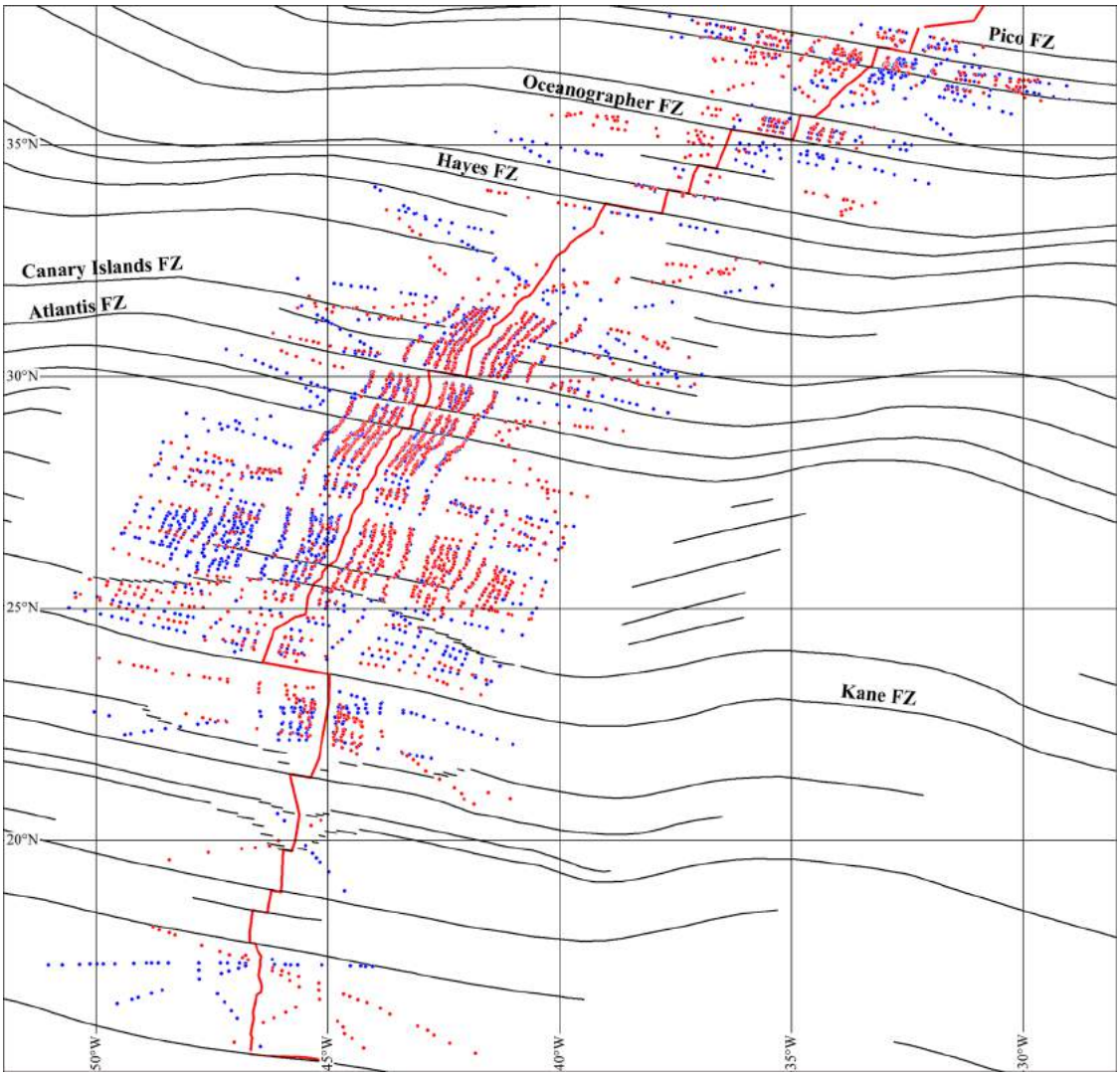

Figure 8. Distribution of magnetic anomaly crossings (blue dots) and reconstructed crossings (red dots) in the central Atlantic.

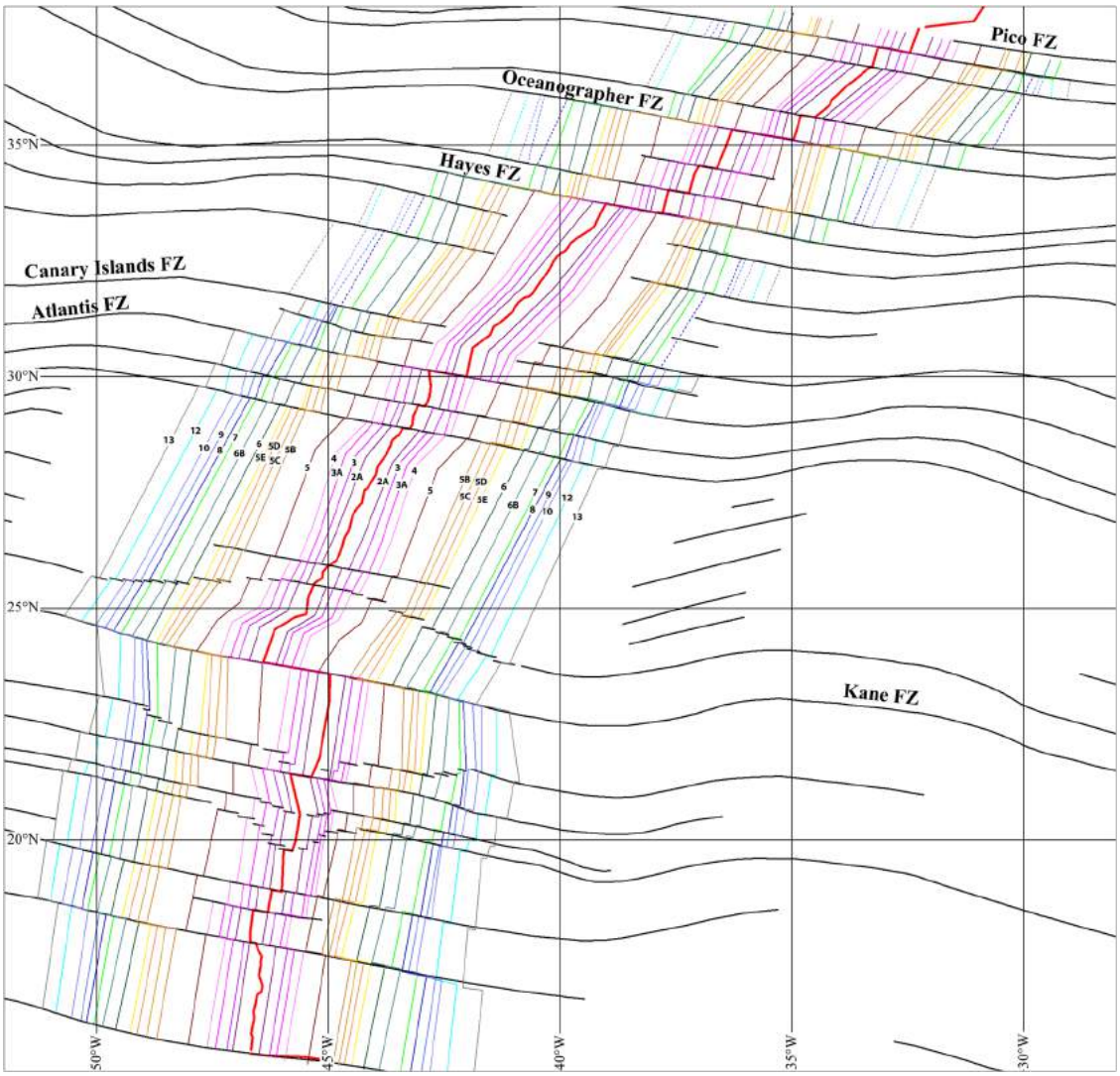

Figure 9. Oligocene to recent isochron chart of the central Atlantic region. Dashed lines represent magnetic lineations.

Table 2. Spreading asymmetry between N. America and northwest Africa since Anomaly 13.

Δx_E An 1 – An 13 (km)	Δx_E An 6 – An 13 (km)	n°	λ (°)	α An 1 – An 13 (per cent)	α An 6 – An 13 (per cent)
457	180	1	30.76	–9.0	–14.4
432	171	2	30.27	–13.9	–18.8
417	155	3	29.75	–16.9	–26.4
424	165	4	29.15	–15.5	–21.6
441	170	5	27.37	–12.1	–19.5
465	187	6	24.72	–7.4	–11.0
484	182	7	24.16	–3.6	–13.5
423	192	8	22.54	–15.7	–8.8
458	193	9	21.02	–8.8	–8.3
448	215	10	19.38	–10.8	+2.1
459	231	11	18.7	–8.6	+9.9
493	240	12	18.14	–1.8	+14.2
513	236	13	17.09	+2.2	+12.1

Notes: Δx_E An 1 – An 13 is the offset of Anomaly 13 along a flow line from the eastern side of the MAR (km). Δx_E An 6 – An 13 is the distance between anomalies 13 and 6 along a flow line from the eastern side of the MAR (km). n° is a segment number. λ is the latitude of the intersection between the selected flow line and the MAR. α An 1 – An 13 is the overall spreading asymmetry since Anomaly 13. α An 6 – An 13 is the spreading asymmetry between anomalies 13 and 6.

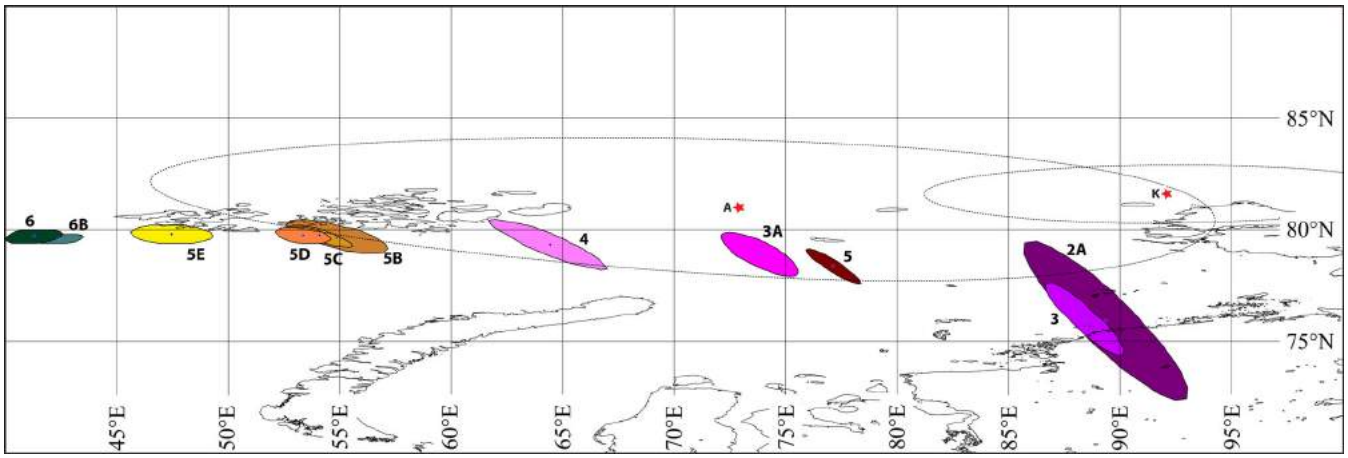

Figure 10. Finite reconstruction poles and confidence ellipses for anomalies 2A, 3, 3A, 4, 5, 5B, 5C, 5D, 5E, 6 and 6B. Red stars 'A' and 'K' show the location of modern Nubia–North America Euler poles of Argus *et al.* (2010) and Kogan & Steblov (2008), respectively, and their confidence ellipses (grey line).

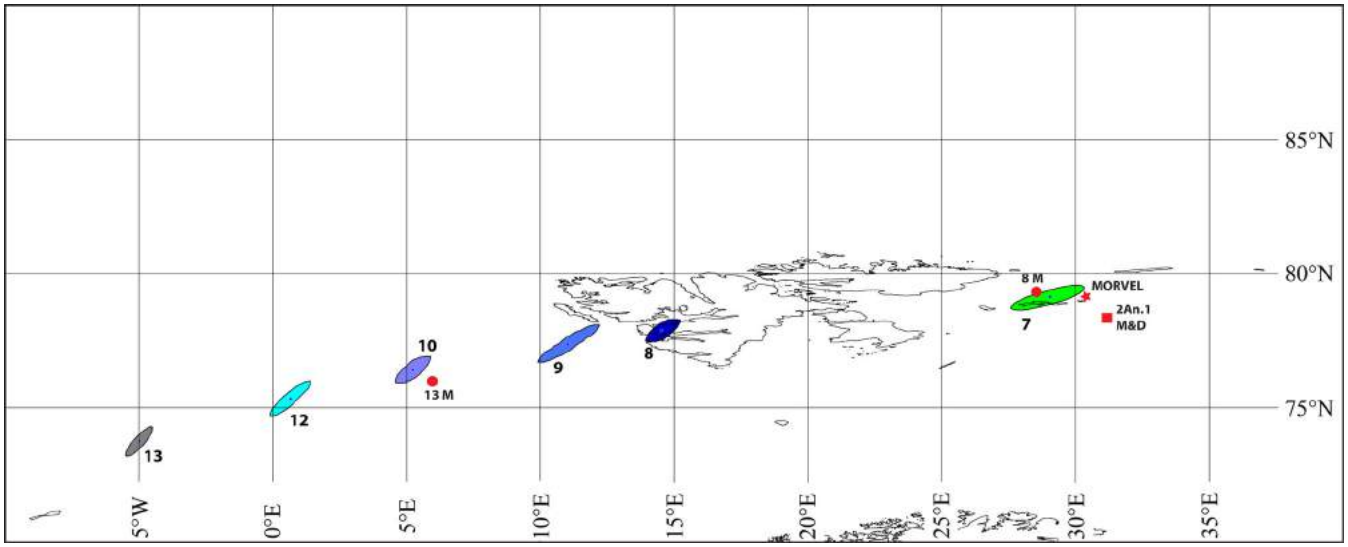

Figure 11. Finite reconstruction poles and confidence ellipses for anomalies 7, 8, 9, 10, 12 and 13. Red star shows the 3-Myr-average MORVEL Nubia–North America pole (DeMets *et al.* 2010). Red square '2An.1 M&D' shows the location of Merkouriev & DeMets (2014) opening pole for Anomaly 2An.1. Red dots '8 M', and '13 M' show the locations of Müller *et al.* (1999) total reconstruction poles for anomalies 8 and 13.

2009). Of course, the latter is the sole possibility that is compatible with geological evidence, as the unique event of compression along the conjugate margins occurred in the Atlas region of northwest Africa, while coeval magmatic activity in the Canary Islands is compatible with a location close to a plate boundary.

5 DISCUSSION

The kinematic model illustrated in the previous sections shows that the North America–northwest Africa motion since 33 Ma is well described by six major stage transitions, at Anomaly 10 (28.3 Ma), 6 (20.1 Ma), 5D (17.3 Ma), 5C (16.0 Ma), 5 (11.0 Ma) and 4 (7.4 Ma) (Fig. 12), accompanied by a quite irregular migration of the stage poles (Fig. 15). It is important to note that while stage pole paths provide important information about the opening history of an ocean basin, the arrangement of a set of finite reconstruction poles such as that shown in Figs 10 and 11 does not contain any kinematic information. It merely shows the location and uncertainty region of the finite reconstruction poles obtained by the statistical analysis of a set of magnetic anomaly crossings and fracture zones. The stage pole path in Fig. 15 and the velocity plot in Fig. 12 show that the time interval between from Anomaly 3 (4.2 Ma) to the present is a single stage. Conversely, although the stage poles between anomalies 5B (14.8 Ma) and 5D (17.3 Ma) are very close each other, the sharp velocity transition at Anomaly 5C (16.0 Ma) implies that they do not form a single stage. Meaningfully, the major stage transition at Anomaly 4, which is also extensively discussed in Merkouriev & DeMets (2014), is synchronous with an abrupt change in the relative motion between North America and Eurasia observed by Merkouriev & DeMets (2008) in the North Atlantic.

A comparison of the result presented here for Anomaly 2A with the GPS-derived Nubia–North America Euler pole from recent studies (Kogan & Steblov 2008; Argus *et al.* 2010) is illustrated in Fig. 10. These two modern Nubia–North America Euler poles are located ∼5.9° and ∼6.0° from our Anomaly 2A pole, respectively. Regarding the average spreading rates along the MAR, these studies predict 21 and 20 mm yr^{-1}, respectively, slower than our average spreading rate corrected for outward displacement, which is 22.14 mm yr^{-1}. Another interesting comparison can be made with

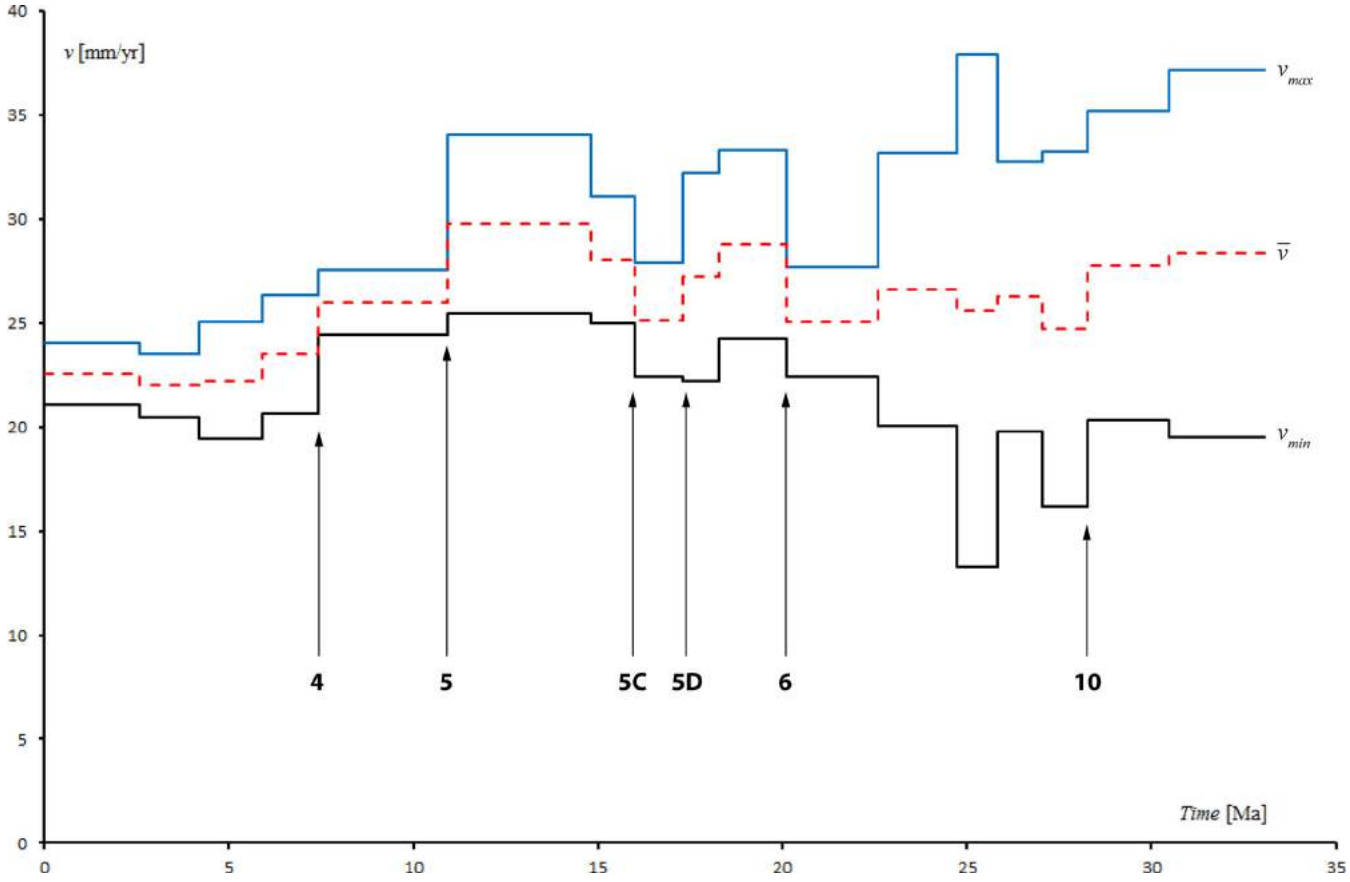

Figure 12. Minimum and maximum spreading rates along the mid-Atlantic Ridge. Six major velocity transitions can be observed at the end of chrons C4 (7.43 Ma), C5r (10.95 Ma), C5C (16.01 Ma), C5D (17.28 Ma), C6r (20.13 Ma) and C10 (28.28 Ma).

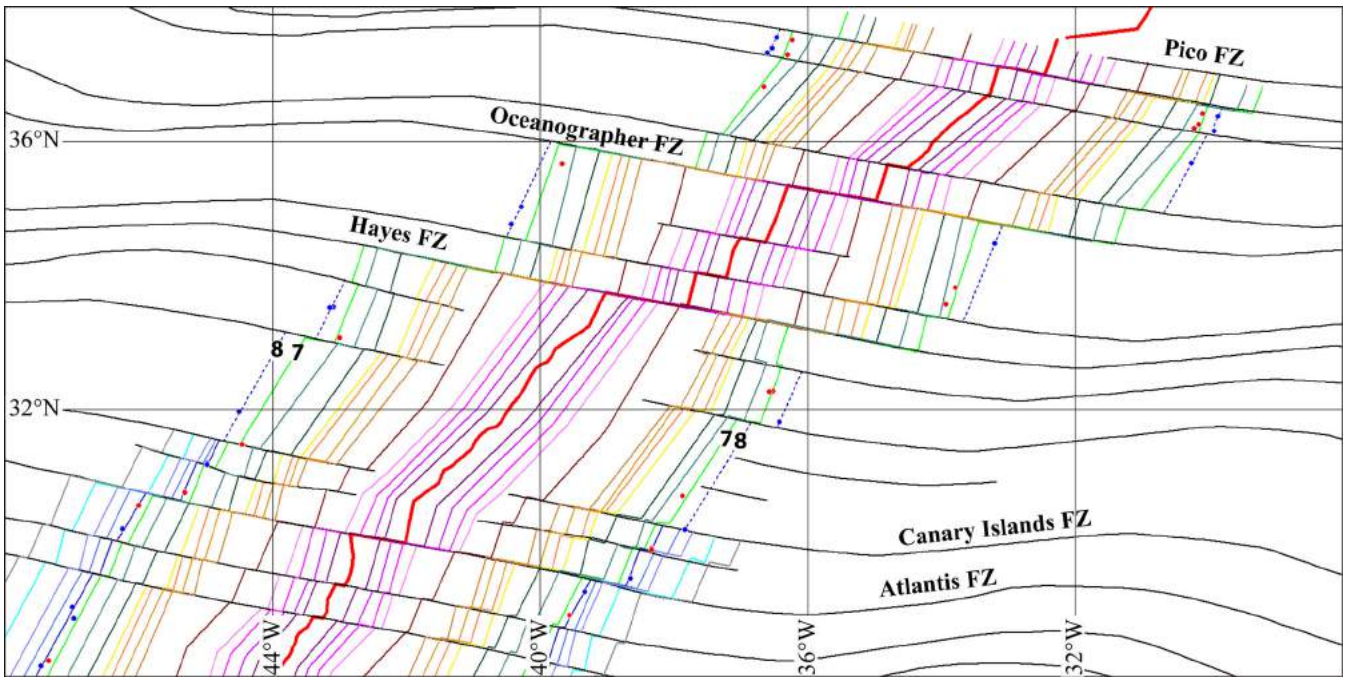

Figure 13. Systematic misfit of reconstructed magnetic crossing associated with Anomaly 8 (red dots) with the corresponding magnetic lineation (dashed blue line).

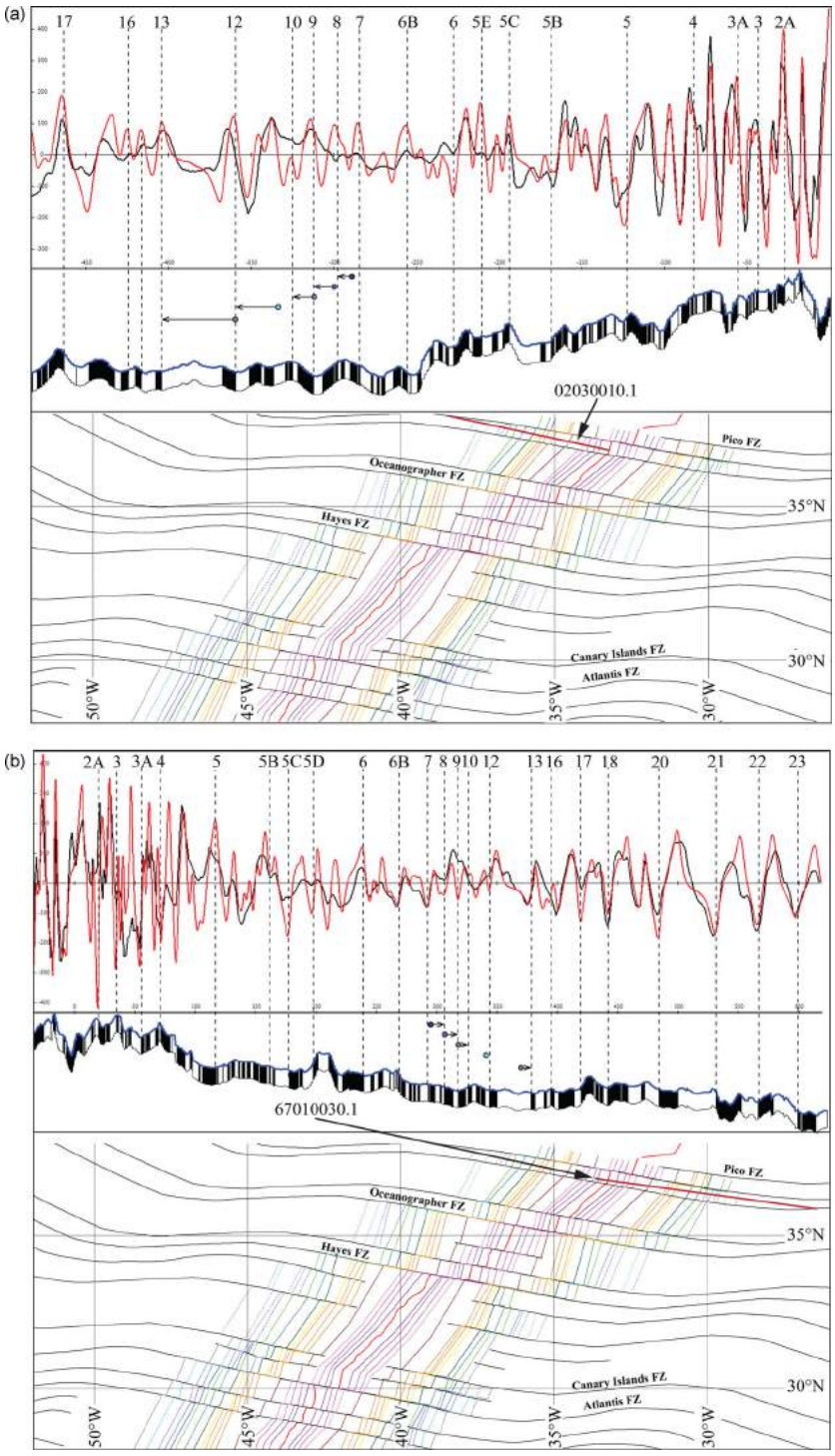

Figure 14. (a) Upper panel: displacement of magnetic crossings older than Anomaly 7 (dots with arrows) in high-quality magnetic profile 02030010.1 north of the CIFZ. The theoretical location of the crossings has been calculated on the basis of the rotation model in Table 1. Lower panel: Location of profile 02030010.1 (red line). (b) Upper panel: displacement of magnetic crossings older than Anomaly 7 (dots with arrows) in high-quality magnetic profile 67010030.1 north of the CIFZ. The theoretical location of the crossings has been calculated on the basis of the rotation model in Table 1. Lower panel: location of profile 67010030.1 (red line). (c) Upper panel: displacement of magnetic crossings older than Anomaly 7 (dots with arrows) in high-quality magnetic profile 67010053.1 north of the CIFZ. The theoretical location of the crossings has been calculated on the basis of the rotation model in Table 1. Lower panel: location of profile 67010053.1 (red line). (d) Upper panel: displacement of magnetic crossings older than Anomaly 7 (dots with arrows) in high-quality magnetic profile 09260004.2 north of the CIFZ. The theoretical location of the crossings has been calculated on the basis of the rotation model in Table 1. Lower panel: location of profile 09260004.2 (red line). (e) Upper panel: displacement of magnetic crossings older than Anomaly 7 (dots with arrows) in high-quality magnetic profile 01030013.1 north of the CIFZ. The theoretical location of the crossings has been calculated on the basis of the rotation model in Table 1. Lower panel: location of profile 01030013.1 (red line). (f) Upper panel: displacement of magnetic crossings older than Anomaly 7 (dots with arrows) in high-quality magnetic profile 15020072.1 north of the CIFZ. The theoretical location of the crossings has been calculated on the basis of the rotation model in Table 1. Lower panel: Location of profile 15020072.1 (red line).

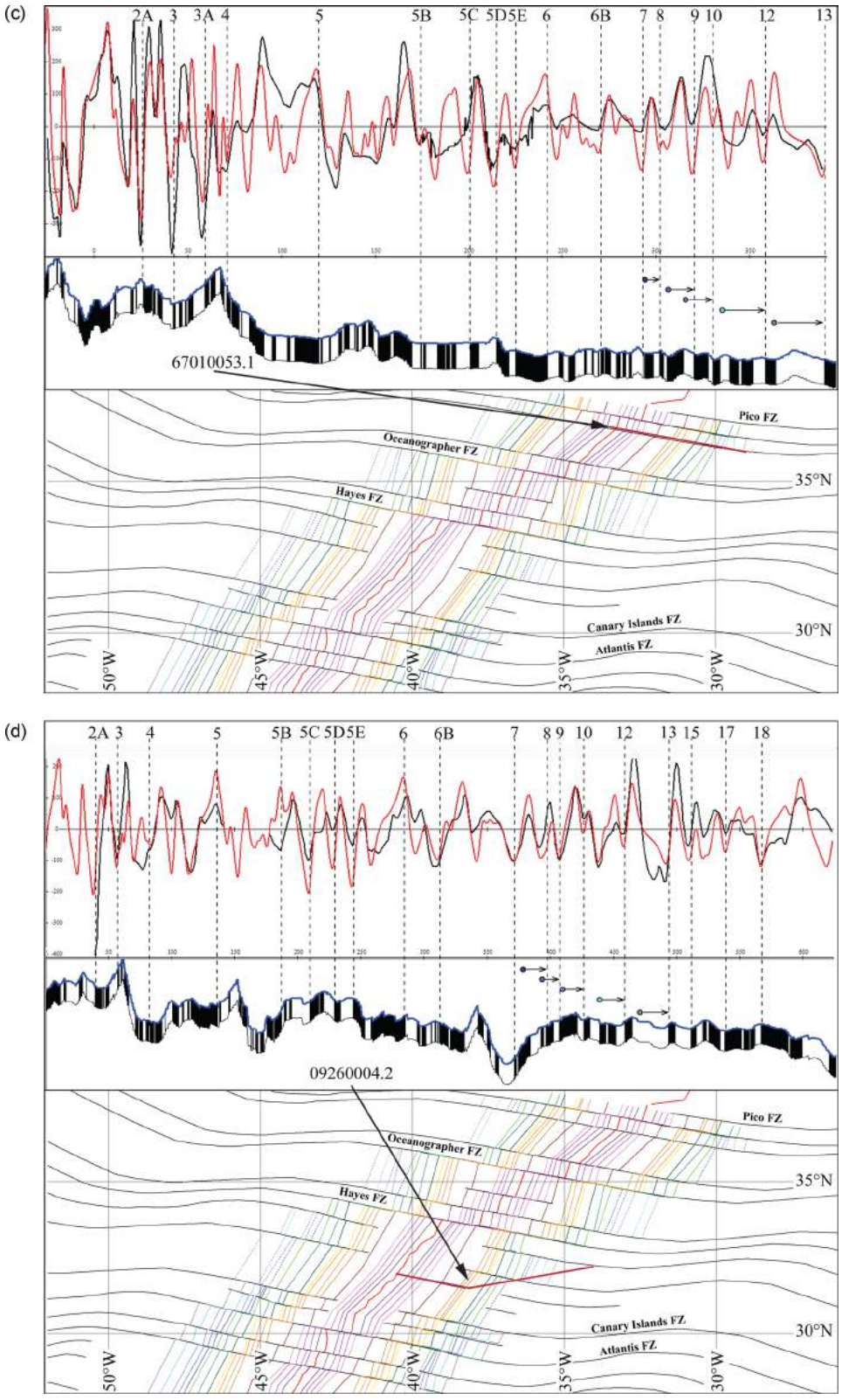

Figure 14 (*Continued.*)

the 3-Myrs-average MORVEL Nubia–North America pole (Fig. 11), which is located at an angular distance of 12.4° with respect to our Anomaly 2A pole, but close to the 2An.1 opening pole of Merkouriev & DeMets (2014), although the average opening rate of 22.9 mm yr^{-1} is not much different from our result.

For the time interval between chrons 8 and 13, which is more relevant for the objectives of this study, we can compare our newly estimated rotations with those obtained by Müller *et al.* (1999). The angular distances between the Müller *et al.* (1999) finite reconstruction poles for anomalies 8 and 13 and our Euler poles are small,

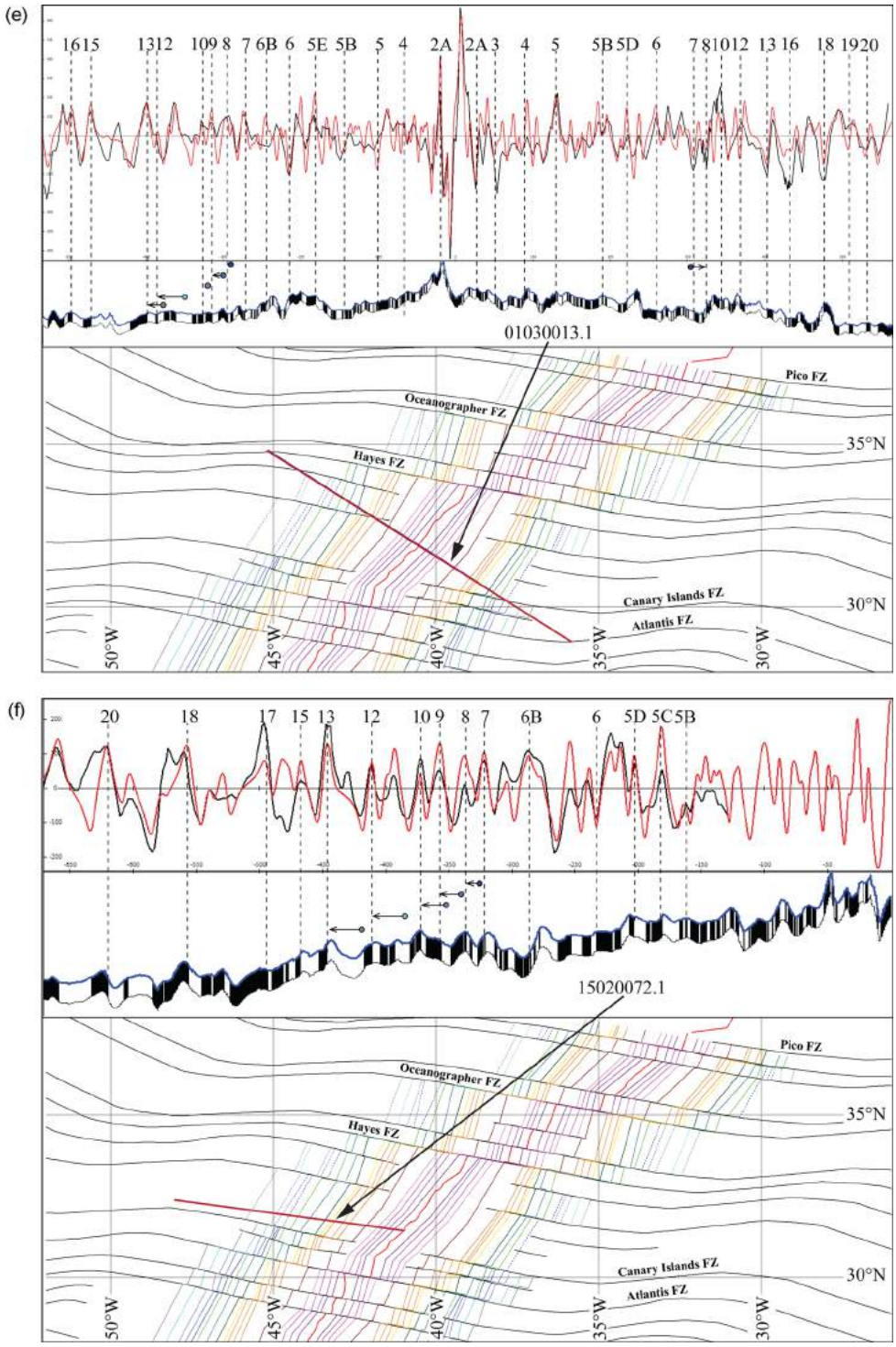

Figure 14 (*Continued.*)

respectively, ∼3° and ∼3.4° (Fig. 11). The average spreading rate predicted by the model of Müller *et al.* (1999) for the time interval from ∼33.1 to ∼26 Ma is 27.08 mm yr^{-1}, which is similar to our estimate of 26.78 mm yr^{-1} (Fig. 12). However we found a major stage transition at Anomaly 10 (28.3 Ma) within the 'canonical' stage bounded by anomalies 13 (33.1 Ma) and 8 (25.8 Ma).

A major feature of the observed distribution of magnetic anomaly crossings older than Anomaly seven time (24.7 Ma) is represented by the misfit with reconstructed crossings in the area north of the CIFZ, which suggests anomalously high spreading rates in the northern part of the central Atlantic. Schettino & Turco (2009) and Schettino *et al.* (2010) interpreted this phenomenon as a consequence of eastward displacement of the lithosphere north of the CIFZ with respect to the northwest African craton, thereby an independent Moroccan Plate would have existed during the Oligocene. However, their conclusions were not supported by a physical model that could explain the elevated spreading rates. Here we show that well-known geodynamic processes in the upper mantle can account

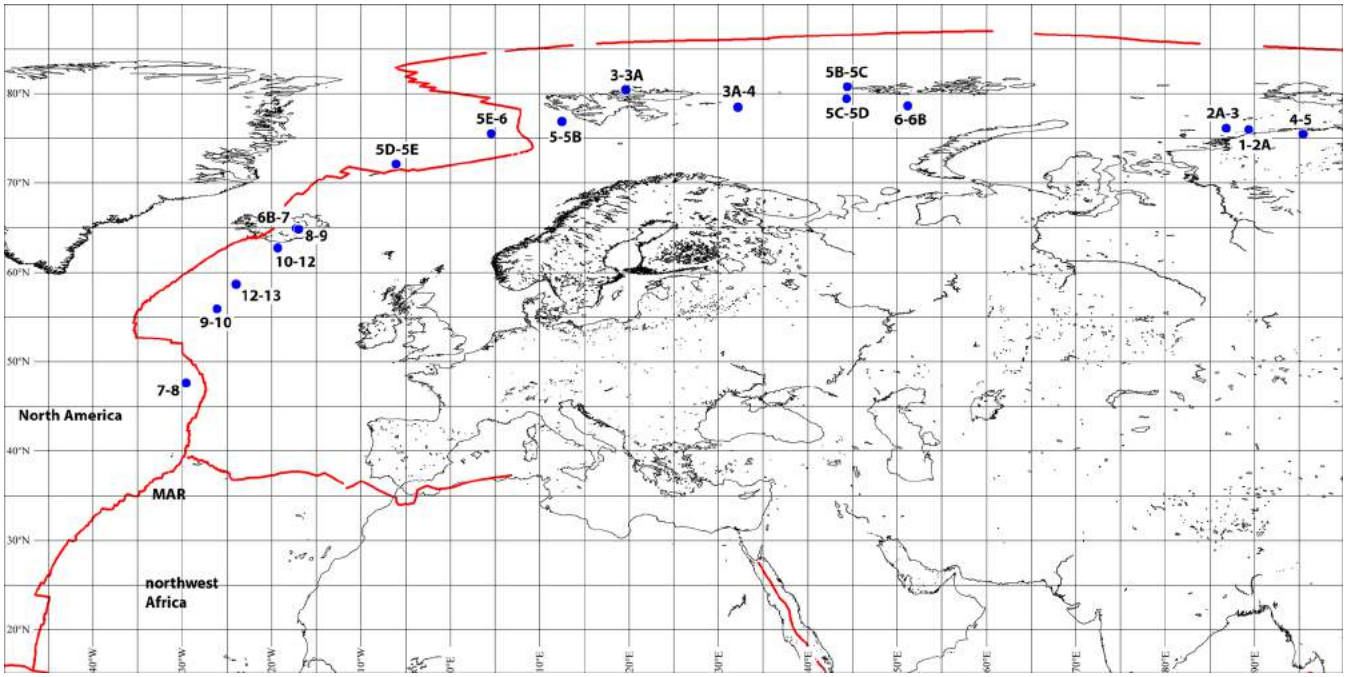

Figure 15. Path of stage poles of North America with respect to northwest Africa since Anomaly 13 (blue dots).

for both the formation of the Atlas mountain belt and the spreading rate anomalies north of the CIFZ.

Let us consider the force balance at a basal point $\boldsymbol{x}$ of a lithospheric plate that moves on the fluid (in rheological sense) asthenosphere. Let $\boldsymbol{\mu}_B$ be the sum of all plate boundary torques, plus torques that are equivalent to boundary forces (e.g. ridge push). If $\boldsymbol{\tau}_B(\boldsymbol{x})$ is the traction exerted at point $\boldsymbol{x}$, associated with this total torque, so that $\boldsymbol{\mu}_B = \boldsymbol{x} \times \boldsymbol{\tau}_B(\boldsymbol{x})$, then the steady equilibrium velocity, $\boldsymbol{v}_0$, at which the plate will move relative to the top transition zone satisfies the equation:

$$\boldsymbol{\tau}_B(\boldsymbol{x}) = \frac{\eta}{h}\boldsymbol{v}_0(\boldsymbol{x}) + \frac{h}{2}\nabla p, \tag{3}$$

where η and h are the average asthenosphere viscosity and thickness, respectively, and ∇p is the lateral pressure gradient in the asthenosphere. The first term at the right-hand side of eq. (3) represents a passive viscous drag, while the second term is an active drag exerted at the base of the lithosphere by a pressure-driven asthenosphere flow in the case of lateral changes in the pressure field (e.g. Schettino 2014). This equation implies that high equilibrium velocities result when $\nabla p \neq 0$ and opposes $\boldsymbol{\tau}_B$. Most importantly, it constrains the local plate velocity $\boldsymbol{v}_0$ given a known system of plate boundary forces and a flow direction in the asthenosphere. Therefore, we can check if this equation can be satisfied by the specific geodynamic and kinematic conditions that existed at the beginning of the Oligocene in the central Atlantic region.

To estimate the traction $\boldsymbol{\tau}_B(\boldsymbol{x})$ associated with plate boundary torques, we note that at the beginning of the Oligocene the African Plate was surrounded by spreading ridges along the eastern, western, and southern boundaries, while an old subduction zone bounded its northeastern side (e.g. Schettino & Turco 2011). The system of spreading ridges around Africa generated a net northward push, which added to the northward slab pull exerted by the Tethyan slab along the northeastern boundary. Therefore, we expect that Africa moved northwards through a counter-clockwise rotation relative to the deep mantle. We can test the tenability of this model considering plate motions in a hot spot frame of reference, which allows to approximate with sufficient accuracy velocities with respect to the more rigid shells formed by the transition zone and the lower mantle. To this purpose, we used an age-recalibrated version of Müller's *et al.* (1993) African fixed hotspot model. In this frame, between 33 and 25 Ma northwest Africa was rotating counter-clockwise about a pole located southwest of the ATJ, as illustrated in Fig. 16. In the hypothesis that an independent Moroccan Plate formed during the Oligocene, we can estimate the velocity field that would have established in the northeastern part of the central Atlantic and in the Moroccan Meseta from the observed spreading rates north of the CIFZ. In fact, we can reasonably assume that during its eastward escape the new plate shared with northwest Africa a common stage pole location S relative to North America, so that the CIFZ was simply converted into a right-lateral strike slip fault without formation of major extensional or compressional structures that have never been observed in the eastern central Atlantic region. The total average misfit of Anomaly 13 crossings north of the CIFZ with respect to isochrons 13 on both sides is ~68 km (left misfit plus right misfit). Therefore, the expected velocity of eastward displacement for the Moroccan Plate is $\delta v = \sim 8.2$ mm yr^{-1} for a time interval $\Delta t = \sim 8.3$ Myr between anomalies 7 and 13. Using the rotation model in Table 1, we easily obtain a stage pole of Morocco relative to North America between 24.73 and 33.06 Ma at $S = (59.15^\circ\text{S}, 150.72^\circ\text{E})$. Therefore, the angular distance of the mid-point of the part of the MAR that lies to the north of the CIFZ from S is $\theta = 154.7^\circ$. This quantity can be used to convert the velocity δv into an angular velocity of eastward displacement, $\delta\omega$:

$$\delta\omega = \frac{180\delta v}{\pi R \sin\theta}. \tag{4}$$

From (4) it results: $\delta\omega = 0.173^\circ$ Myr^{-1}. Consequently, the total angular displacement for the time interval Δt is: $\Delta\Omega = \delta\omega\Delta t = 1.44^\circ$. From this quantity, we can calculate a stage pole of Morocco relative to North America for the time interval between Anomalies 7 and 13. The corresponding velocity field relative to the deep mantle

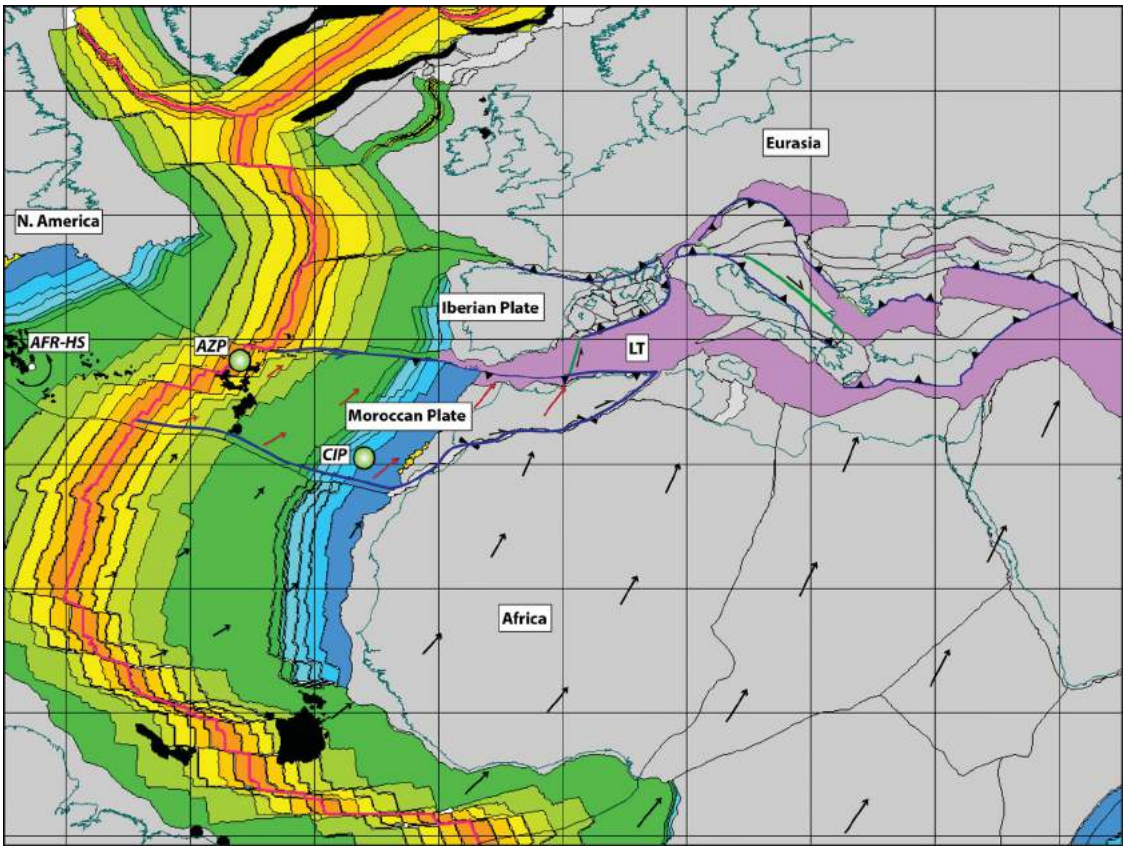

Figure 16. Plate reconstruction at 33.1 Ma (early Oligocene), showing a possible configuration of plate boundaries in the central Atlantic and western Mediterranean. Grey, Continental lithosphere; Light grey, Extended continental crust; Purple, Mesozoic oceanic crust of the Tethyan domain; LT, Ligurian Tethys; AZP, Azores plume location; CIP, Canary Islands plume; white circle indicates the location of the African instantaneous Euler pole in a hot spot reference frame; red arrows represent absolute velocity field of the Moroccan Plate and direction of asthenosphere toroidal flow; Black arrows show the absolute motion of Africa.

is shown in Fig. 16. By eq. (3), this field is compatible with both an excess ridge push from mantle plumes that could have existed in the northern central Atlantic and an ENE directed upper mantle Poiseuille–Couette viscous flow associated with lateral pressure variations.

Many lines of evidence indicate that the location of the Azores plume at the beginning of the Oligocene (∼33 Ma) was more to the south and did not coincide with the present day location of the Azores plateau (Gente *et al.* 2003). At that time, the latter did not exist yet, but excess volcanism between the Atlantis Seamount and the MAR between 40 and 25 Ma and anomalously shallow depths in the residual topography suggest that an ancestor of the Azores mantle plume existed close to the MAR segments facing the Moroccan Meseta, south of the Pico FZ (Fig. 16). Numerical modelling shows that in normal conditions ridges generate compressive deviatoric stress fields of ∼40 MPa in the elastic zone of the oceanic lithosphere, which are independent from the spreading velocity (Bott 1991). However, anomalous hot and low-density upper mantle zones beneath oceanic ridges, forming ocean floor swells, determine a substantial increase in the magnitude of the compressional deviatoric stress field in the oceanic area, reaching 100 MPa beneath the oldest crust, and the appearance of a significant compressional deviatoric component (up to 90 MPa) in the adjacent continental margin (Bott 1991). Therefore, there is evidence that an elevated and uncompensated ridge push component operated in the time interval before 25 Ma in the area north of the CIFZ. This force field was directed eastwards in the eastern sector of the central Atlantic.

The existence of an Oligocene ENE directed toroidal flow in the upper mantle, which would have exerted active drag at the base of the Moroccan lithosphere determining higher spreading rates along the MAR, cannot be proved directly. The effect of asthenosphere currents on geological processes has been studied by several authors, notably King & Anderson (1998), Alvarez (2010), Faccenna & Becker (2010), Becker & Faccenna (2011). In the case of the northwest African craton, Duggen *et al.* (2009) first postulated the existence of an asthenosphere flow from the Canary Islands mantle plume (Anguita & Hernan 2000) toward the western Mediterranean region, which travelled through a sublithospheric channel beneath the Moroccan Meseta and was responsible for voluminous Neogene volcanism in the Atlas region. It is interesting to note that according to Missenard & Cadoux (2012) the time interval between ∼35 and ∼11 Ma was characterized by the absence of volcanism in this area, thereby apparently an asthenosphere flow beneath the Moroccan Meseta during the Oligocene–early Miocene should be excluded. However, we stress the fact that volcanism is always controlled by the onset of extensional regime on a pre-existing system of fractures and faults, not by the mere existence of thermal anomalies (Anderson & Natland 2005). Before 35 Ma, the Canary Islands mantle plume already existed, and it is likely that a weak flow formed beneath the Atlas Rift and directed towards the Mediterranean subduction zones, giving rise to magmatic episodes with

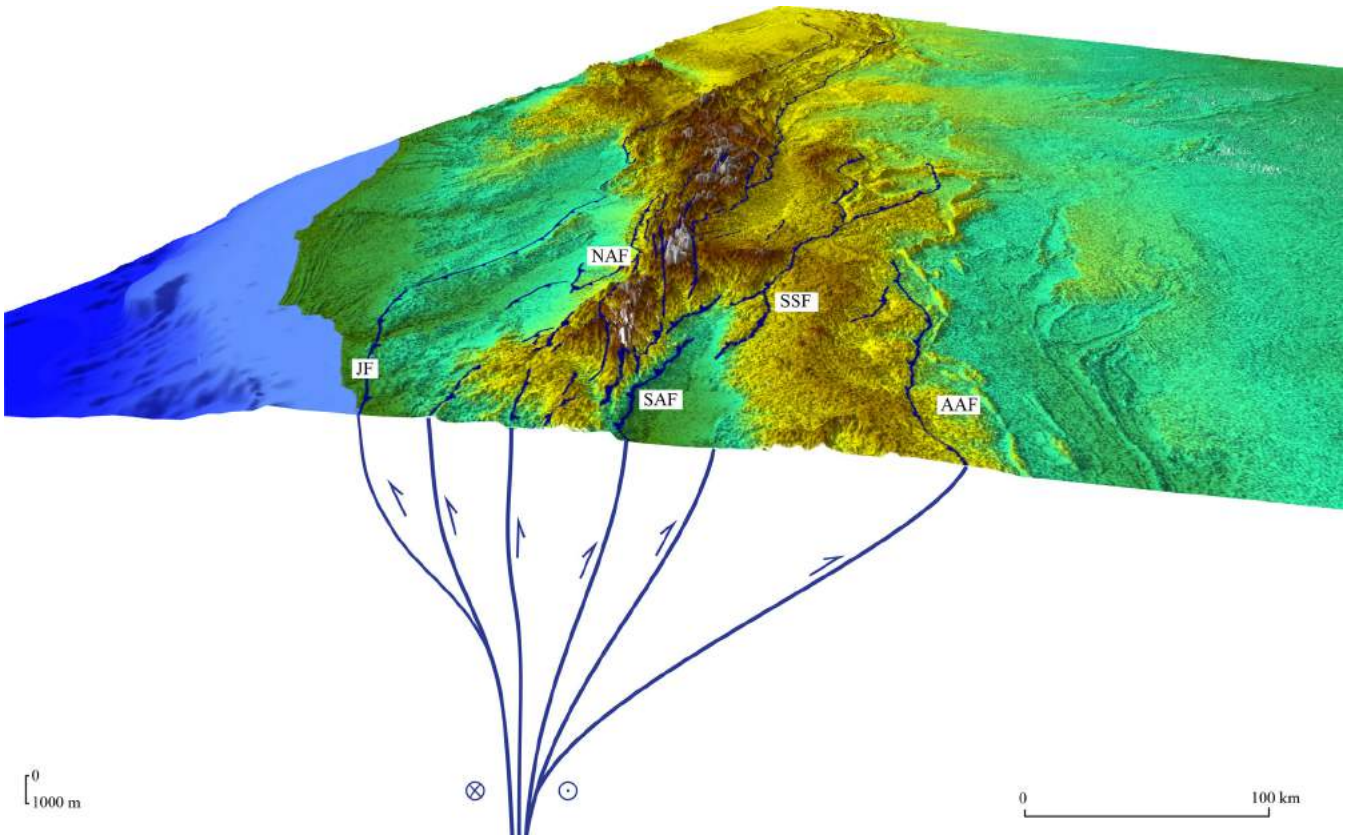

Figure 17. Structural interpretation of the Atlas mountain belt as a giant flower structure. JF, Jebilet Fault; SAF, South Atlas Fault; NAF, North Atlas Fault; AAF, Anti Atlas Fault; SSF, South Siroua Fault.

limited amount of alkaline volcanism (Missenard & Cadoux 2012). Here we suggest that rapid flow capable of triggering intracontinental deformation started only at the beginning of the Oligocene, when the high-pressure region close to the plume was faced by a low-pressure zone in the western Mediterranean, associated with the southward subduction of Ligurian Tethys lithosphere beneath Morocco (Fig. 16; Vergés & Fernàndez 2012). In this scenario, the combined effect of excess ridge push from the Azores plume and negative pressure gradients in the region between the Canary Islands plume and the western Mediterranean drove the inversion of the Atlas rift structures. Such transpressional tectonic regime hampered the upwelling of magma until the end of the Rif–Tell orogeny in the Neogene.

The hypothetical scenario illustrated above implies that a Moroccan Plate formed as a consequence of the combined effect of excess ridge push from mantle plumes and active eastward traction exerted by the asthenosphere. In this instance, the Atlas mountain belt should be interpreted as a giant flower structure associated with transpressional motion along the South Atlas Fault (Fig. 17) and not as an intracontinental chain generated by isostasy or dynamic topography (e.g. Teixell *et al.* 2003). There is general consensus that the inversion of the Mesozoic structures of the Atlas rift (e.g. Le Roy and Piqué 2001), which led to the formation of the Atlas orogen (Beauchamp *et al.* 1996; Frizon de Lamotte *et al.* 2000; Piqué *et al.* 2002), occurred during the Oligocene–early Miocene time interval. Therefore, the timing of the Atlas orogeny is coeval with the high spreading rate event observed in the northern part of the central Atlantic. In the classic central Atlantic kinematic models, the amount of deformation in the Atlas region is considered negligible, so that it is assumed that northwest Africa behaved as a single rigid plate both during the break-up of Pangea and the Cenozoic phase of Atlas orogeny (e.g. Klitgord & Schouten 1986; Roest *et al.* 1992). Conversely, in the model of Schettino & Turco (2009), an independent Moroccan Plate existed during the Triassic–early Jurassic between North America, northwest Africa, and Iberia. At that time, a wide rift formed between the Moroccan Meseta and the African craton. Later, during the Cenozoic, the rift structures were inverted as a consequence of eastward transpressional motion between the Moroccan Plate and northwest Africa. Although this view has been challenged by Labails *et al.* (2010), there is strong geological evidence of dextral transpression both in the High Atlas and in the Anti-Atlas (Courbouleix *et al.* 1981; Weijermars 1993; Gomez *et al.* 1998; Malusà *et al.* 2007; Ellero *et al.* 2012). Therefore, the argument that the amount of shortening in the Atlas is moderate (e.g. Teixell *et al.* 2003) cannot be used to support a rigid-plate approximation for northwest Africa during the Oligocene.

6 CONCLUSIONS

In this paper, we have performed a high-resolution kinematic analysis of the central Atlantic region since the Oligocene (~33 Ma) through a detailed analysis of marine magnetic and gravity data. The main objective was to detect the existence of minor changes in plate motions during the last 33 Myr within the 'canonical' stages bounded by anomalies 6, 8 and 13. We have shown that at least seven stages are necessary to describe the sea floor spreading history between North America and northwest Africa since 33 Ma, with

boundaries at Anomaly 10 (28.3 Ma), 6 (20.1 Ma), 5D (17.3 Ma), 5C (16.0 Ma), 5 (11.0 Ma) and 4 (7.4 Ma). Another important objective was to describe ridge kinematics along the central Atlantic part of the MAR. We have found that some ridge segments were subject to coalescence, others to reorientation, while spreading segment splitting through formation of small-offset transform faults was quite common in this region. Finally, we have described a geodynamic scenario that could explain the high spreading rates observed in the northern part of the central Atlantic. This model implies the formation of an independent tectonic plate during the Oligocene, namely the Moroccan Plate, which decoupled the oceanic lithosphere north of the CIFZ from northwest Africa and moved in dextral transpression along the former Atlas Rift, determining structural inversion building of the Atlas mountain belt.

ACKNOWLEDGEMENTS

The GEODAS ship-track data used in this study can be found at NGDC (http://www.ngdc.noaa.gov/mgg/geodas/trackline.html). The computer program used in the analysis of magnetic data was designed by the first author and can be freely downloaded at: http://www.serg.unicam.it/Downloads.htm. We would like to thank J. Dyment and an anonymous reviewer for their useful suggestions.

REFERENCES

Alvarez, W., 2010. Protracted continental collisions argue for continental plates driven by basal traction, *Earth planet. Sci. Lett.,* **296,** 434–442.

Anderson, D.L. & Natland, J.H., 2005. A brief history of the plume hypothesis and its competitors: concept and controversy, in *Plates, Plumes, and Paradigms,* pp. 119–145, eds Foulger, G.R., Natland, J.H., Presnall, D.C. & Anderson, D.L., Geological Society of America Special Paper 388.

Anguita, F. & Hernan, F., 2000. The Canary Islands origin: a unifying model, *J. Volc. Geother. Res.,* **103,** 1–26.

Argus, D.F., Gordon, R.G., Heflin, M.B., Ma, C., Eanes, R., Willis, P., Peltier, W.R. & Owen, S.E., 2010. The angular velocities of the plates and the velocity of Earth's centre from space geodesy, *Geophys. J. Int.,* **180**(3), 913–960.

Beauchamp, W., Barazangi, M., Demnati, A. & El Alji, M., 1996. Intracontinental Rifting and Inversion: Missour Basin and Atlas Mountains, Morocco, *AAPG Bull.,* **80**(9), 1459–1482.

Becker, T.W. & Faccenna, C., 2011. Mantle conveyor beneath the Tethyan collisional belt, *Earth planet. Sci. Lett.,* **310,** 453–461.

Bott, M.H.P., 1991. Ridge push and associated plate interior stress in normal and hot spot regions, *Tectonophysics,* **200**(1–3), 17–32.

Cande, S.C. & Kent, D.V., 1995. Revised calibration of the geomagnetic polarity timescale for the late Cretaceous and Cenozoic, *J. geophys. Res.,* **100**(B4), 6093–6095.

Courbouleix, S., Delpont, G. & Destaucq, C., 1981. Un grand décrochement Est-Ouest au Nord du Maroc, à l'origine des structures plissées atlasiques. Arguments géologiques et expérimentaux, *Bull. Soc. Geol. France,* **23**(1), 33–43.

DeMets, C. & Wilson, D.S., 2008. Toward a minimum change model for recent plate motions: calibrating seafloor spreading rates for outward displacement, *Geophys. J. Int.,* **174**(3), 825–841.

DeMets, C., Gordon, R.G. & Argus, D.F., 2010. Geologically current plate motions, *Geophys. J. Int.,* **181,** 1–80.

Duggen, S., Hoernle, K.A., Hauff, F., Kluegel, A., Bouabdellah, M. & Thirlwall, M.F., 2009. Flow of Canary mantle plume material through a subcontinental lithospheric corridor beneath Africa to the Mediterranean, *Geology,* **37**(3), 283–286.

Ellero, A., Ottria, G., Ouanaimi, H. & Malusà, M.G., 2012. Structural geological analysis of the High Atlas (Morocco): evidences of a transpressional fold-thrust belt, in *Tectonics - Recent Advances,* eds Sharkov, E., INTECH, Open Access Publisher.

Escartín, J., Cannat, M., Pouliquen, G., Rabain, A. & Lin, J., 2001. Crustal thickness of V-shaped ridges south of the Azores: interaction of the Mid-Atlantic Ridge (36°–39°N) and the Azores hot spot, *J. geophys. Res.,* **106**(B10), 21 719–21 735.

Faccenna, C. & Becker, T.W., 2010. Shaping mobile belts by small-scale convection, *Nature,* **465**(7298), 602–605.

Francheteau, J., 1973. Plate tectonics model of the opening of the Atlantic Ocean south of the Azores, in *Implications of Continental Drift to the Earth Sciences,* pp. 197–202, eds Tarling, D.H. & Runcorn, S.K., Academic Press.

Frizon de Lamotte, D., Saint Bezar, B., Bracène, R. & Mercier, E., 2000. The two main steps of the Atlas building and geodynamics of the western Mediterranean, *Tectonics,* **19**(4), 740–761.

Gente, P. *et al.*, 1995. Characteristics and evolution of the segmentation of the Mid-Atlantic Ridge between 20°N and 24°N during the last 10 million years, *Earth planet. Sci. Lett.,* **129**(1), 55–71.

Gente, P., Dyment, J., Maia, M. & Goslin, J., 2003. Interaction between the Mid-Atlantic Ridge and the Azores hot spot during the last 85 Myr: emplacement and rifting of the hot spot-derived plateaus, *Geochem. Geophys. Geosyst.,* **4,** 8514, doi:10.1029/2003GC000527.

Gomez, F., Allmendinger, R., Barazangi, M., Er-Raji, A. & Dahmani, M., 1998. Crustal shortening and vertical strain partitioning in the Middle Atlas Mountains of Morocco, *Tectonics,* **17**(4), 520–533.

Hafid, M., Zizi, M., Bally, A.W. & Salem, A.A., 2006. Structural styles of the western onshore and offshore termination of the High Atlas, Morocco, *Comptes Rendus Geosci.,* **338**(1), 50–64.

Heirtzler, J.R., Dickson, G.O., Herron, E.M., Pitman III, W.C. & Le Pichon, X., 1968. Marine magnetic anomalies, geomagnetic field reversals, and motions of the ocean floor and continents, *J. geophys. Res.,* **73**(6), 2119–2136.

Hellinger, S.J., 1981. The uncertainties of finite rotations in plate tectonics, *J. geophys. Res.,* **86,** 9312–9318.

Hey, R., 1977. A new class of "pseudofaults" and their bearing on plate tectonics: a propagating rift model, *Earth planet. Sci. Lett.,* **37**(2), 321–325.

Jones, S. M., White, N. & Maclennan, J., 2002. V-shaped ridges around Iceland: Implications for spatial and temporal patterns of mantle convection, *Geochem. Geophys. Geosyst.,* **3**(10), 1059, doi:10.1029/2002GC000361.

King, S.D. & Anderson, D.L., 1998. Edge-driven convection, *Earth planet. Sci. Lett.,* **160,** 289–296.

Kleinrock, M.C., Tucholke, B.E., Lin, J. & Tivey, M.A., 1997. Fast rift propagation at a slow-spreading ridge, *Geology,* **25**(7), 639–642.

Klitgord, K.D. & Schouten, H., 1986. Plate kinematics of the central Atlantic, in *The Geology of North America,* Vol. M: The Western North Atlantic Region, pp. 351–378, eds Vogt, P.R. & Tucholke, B.E., Geol. Soc. of America.

Kogan, M.G. & Steblov, G.M., 2008. Current global plate kinematics from GPS (1995-2007) with the plate-consistent reference frame, *J. geophys. Res.,* **113,** B04416, doi:10.1029/2007JB005353.

Labails, C., Olivet, J.L., Aslanian, D. & Roest, W.R., 2010. An alternative early opening scenario for the Central Atlantic Ocean, *Earth planet. Sci. Lett.,* **297**(3), 355–368.

Le Pichon, X. & Fox, J.P., 1971. Marginal offsets, fracture zones, and the early opening of the North Atlantic, *J. geophys. Res.,* **76,** 6294–6308.

Le Roy, P. & Piqué, A., 2001. Triassic-Liassic Western Moroccan synrift basins in relation to the Central Atlantic opening, *Mar. Geol.,* **172,** 359–381.

Malusà, M.G., Polino, R., Cerrina Feroni, A., Ellero, A., Ottria, G., Baidder, L. & Musumeci, G., 2007. Post-Variscan tectonics in eastern Anti-Atlas (Morocco), *Terra Nova,* **19,** 481–489.

Matias, L.M., Olivet, J.L., Aslanian, D. & Fidalgo, L., 2005. PLACA: a white box for plate reconstruction and best-fit pole determination, *Comput. Geosci.,* **31**(4), 437–452.

Matthews, K.J., Müller, R.D., Wessel, P. & Whittaker, J.M., 2011. The tectonic fabric of the ocean basins, *J. geophys. Res.,* **116,** B12109, doi:10.1029/2011JB008413.

Merkouriev, S. & DeMets, C., 2008. A high-resolution model for Eurasia–North America plate kinematics since 20 Ma, *Geophys. J. Int.,* **173**(3), 1064–1083.

Merkouriev, S. & DeMets, C., 2014. High-resolution estimates of Nubia–North America plate motion: 20 Ma to present, *Geophys. J. Int.,* **196**(3), 1281–1298.

Missenard, Y. & Cadoux, A., 2012. Can Moroccan Atlas lithospheric thinning and volcanism be induced by Edge-Driven Convection?, *Terra Nova,* **24**(1), 27–33.

Müller, R.D. & Roest, W.R., 1992. Fracture zones in the North Atlantic from combined Geosat and Seasat data, *J. geophys. Res.,* **97**(B3), 3337–3350.

Müller, R.D., Royer, J.-Y. & Lawver, L.A., 1993. Revised plate motions relative to the hotspots from combined Atlantic and Indian Ocean hotspot tracks, *Geology,* **21**(3), 275–278.

Müller, R.D., Roest, W.R., Royer, J.-Y., Gahagan, L.M. & Sclater, J.G., 1997. Digital isochrons of the world's ocean floor, *J. geophys. Res.,* **102**(B2), 3211–3214.

Müller, R.D., Royer, J.-Y., Cande, S.C., Roest, W.R. & Maschenkov, S., 1999. New constraints on the Late Cretaceous/Tertiary plate tectonic evolution of the Caribbean, in *Caribbean Basins, Sedimentary Basins of the World,* Vol. 4, pp. 33–59, ed. Mann, P., Elsevier Science B.V.

Olivet, J.L., Bonnin, J., Beuzart, P. & Auzende, J.M., 1984. Cinématique de l'Atlantique nord et central, *Rapp. Sci. Tech.,* **54,** Centre National pour l'Exploration des Oceans, 108–112.

Piqué, A., Tricart, P., Guiraud, R., Laville, E., Bouaziz, S., Amrhar, M. & Ouali, R.A., 2002. The Mesozoic–Cenozoic Atlas belt (North Africa): an overview, *Geodinamica Acta,* **15,** 185–208.

Pitman III, W.C & Talwani, M., 1972. Sea floor spreading in the North Atlantic, *Geol. Soc. Am. Bull.,* **83**(3), 619–646.

Roest, W.R., Dañobeitia, J.J., Verhoef, J. & Collette, B.J., 1992. Magnetic anomalies in the Canary basin and the Mesozoic evolution of the central North Atlantic, *Mar. geophys. Res.,* **14**(1), 1–24.

Rona, P.A., 1976. Asymmetric fracture zones and sea-floor spreading. *Earth planet. Sci. Lett.,* **30**(1), 109–116.

Rona, P.A. & Gray, D.F., 1980. Structural behavior of fracture zones symmetric and asymmetric about a spreading axis: Mid-Atlantic Ridge (latitude 23 N to 27 N), *Geol. Soc. Am. Bull.,* **91**(8), 485–494.

Sandwell, D.T., Müller, R.D., Smith, W.H., Garcia, E. & Francis, R., 2014. New global marine gravity model from CryoSat-2 and Jason-1 reveals buried tectonic structure, *Science,* **346**(6205), 65–67.

Schettino, A., 2012. Magan: a new approach to the analysis and interpretation of marine magnetic anomalies, *Comput. Geosci.,* **39,** 135–144.

Schettino, A., 2014. *Quantitative Plate Tectonics,* Springer, 403 pp.

Schettino, A. & Scotese, C.R., 2005. Apparent polar wander paths for the major continents (200 Ma - Present Day): a paleomagnetic reference frame for global plate tectonic reconstructions, *Geophys. J. Int.,* **163**(2), 727–759.

Schettino, A. & Turco, E., 2009. Breakup of Pangaea and plate kinematics of the central Atlantic and Atlas regions, *Geophys. J. Int.,* **110,** 1078–1097.

Schettino, A. & Turco, E., 2011. Tectonic history of the western Tethys since the late Triassic, *GSA Bull.,* **123**(1/2), 89–105.

Schettino, A., Tassi, L. & Turco, E., 2010. Reply to comments by C. Labails and W. Roest on 'Breakup of Pangaea and plate kinematics of the central Atlantic and Atlas regions', *Geophys. J. Int.,* **183,** 99–102.

Schouten, H., Dick, H.J.B. & Klitgord, K.D., 1987. Migration of mid-ocean-ridge volcanic segments, *Nature,* **326,** 835–839.

Sclater, J.G., Hellinger, S. & Tapscott, C., 1977. Paleobathymetry of the Atlantic Ocean from the Jurassic to the present, *J. Geol.,* **85**(5), 509–552.

Sundvik, M.T. & Larson, R.L., 1988. Seafloor spreading history of the western North Atlantic Basin derived from the Keathley sequence and computer graphics, *Tectonophysics,* **155**(1–4), 49–71.

Teixell, A., Arboleya, M.L., Julivert, M. & Charroud, M., 2003. Tectonic shortening and topography in the central High Atlas (Morocco), *Tectonics,* **22**(5), doi:10.1029/2002TC001460.

Vergés, J. & Fernàndez, M., 2012. Tethys–Atlantic interaction along the Iberia–Africa plate boundary: the Betic–Rif orogenic system, *Tectonophysics,* **579,** 144–172.

Vogt, P.R., 1971. Asthenosphere motion recorded by the ocean floor south of Iceland, *Earth planet. Sci. Lett.,* **13,** 153–160.

Weijermars, R., 1993. Estimation of paleostress orientation within deformation zones between two mobile plates, *GSA Bull.,* **105**(11), 1491–1510.

White, R.S., 1997. Rift–plume interaction in the North Atlantic, *Phil. Trans. R. Soc. Lond., A,* **355**(1723), 319–339.

SUPPORTING INFORMATION

Additional Supporting Information may be found in the online version of this paper:

Figure S1.
(http://gji.oxfordjournals.org/lookup/suppl/doi:10.1093/gji/ggw022/-/DC1).

Please note: Oxford University Press is not responsible for the content or functionality of any supporting materials supplied by the authors. Any queries (other than missing material) should be directed to the corresponding author for the paper.